J. Fluid Mech. (1978), *vol.* 88, *part* 3, *pp.* 401–430
Printed in Great Britain

The large-scale structure of unsteady self-similar rolled-up vortex sheets

By D. I. PULLIN

Department of Mechanical Engineering, University of Melbourne, Parkville, Victoria 3052, Australia

(Received 22 September 1977 and in revised form 17 February 1978)

Two problems involving the unsteady motion of two-dimensional vortex sheets are considered. The first is the roll-up of an initially plane semi-infinite vortex sheet while the second is the power-law starting flow past an infinite wedge with separation at the wedge apex modelled by a growing vortex sheet. In both cases well-known similarity solutions are used to transform the time-dependent problem for the sheet motion into an integro-differential equation. Finite-difference numerical solutions to these equations are obtained which give details of the large-scale structure of the rolled-up portion of the sheet. For the semi-infinite sheet good agreement with Kaden's asymptotic spiral solution is obtained. However, for the starting-flow problem distortions in the sheet shape and strength not predicted by the leading-order asymptotic solutions were found to be significant.

1. Introduction

The mechanics of unsteady two-dimensional vortex sheets are of fundamental importance in obtaining an understanding of the large-scale behaviour of two-dimensional and quasi-three-dimensional thin shear layers in a variety of fluid-mechanical applications. Examples are the much studied case of the roll-up of the approximately two-dimensional shear layer shed by a high aspect ratio wing, the unsteady separated flow past a sharp-edged body, and the nonlinear Kelvin–Helmholtz instability. In these and other examples, the vortex sheet is usually regarded as the infinite Reynolds number limit in which the thin shear layer is contracted into a two-dimensional line distribution of circulation, all points of which convect with the local flow velocity in an otherwise irrotational fluid. The problem is then to solve the initial-value problem describing the vortex-sheet motion and, since the governing equation is nonlinear [see (2)], this task must usually be performed numerically.

Over the past few decades a large number of attempts have been made (see Fink & Soh (1974) for a comprehensive review) to model the vortex-sheet motion by that of a finite number of point vortices whose initial strengths and positions represent a discretized model of the distributed sheet circulation. Although partly successful, these calculations usually resulted in unphysical chaotic motion of the vortices after some initial period of more or less coherent motion. After a careful analysis, Fink & Soh (1974) concluded that a point-vortex representation implicitly involves the neglect of logarithmic terms which represent the local contribution in the Cauchy principal-value integrals for the self-induced velocity field of a vortex sheet proper.

They argue that the logarithmic terms, although initially vanishingly small, amplify through small sheet distortions, leading eventually to the chaotic motion observed by most authors. The remedy proposed is to rediscretize the sheet at every time step by replacing the current vortex set with another equidistantly spaced set of the same total circulation. This appears to check the growth of the logarithmic error, hence inhibiting the onset of chaotic motion. In several applications, including the problem of the finite vortex sheet, Fink & Soh (1974, 1978) obtained smooth vortex-sheet behaviour which included coherent spiral roll-up over longer periods than had previously been reported.

There are several interesting cases, however, for which, through the absence of appropriate length and circulation scales, the vortex-sheet motion admits similarity solutions. It is then possible to formulate the problem as an integro-differential equation which does not contain time explicitly, and thereby avoid difficulties directly associated with unsteadiness. Apart from their intrinsic interest, the similarity flows may then serve as useful basic solutions for the time-dependent calculation methods and at the same time provide starting conditions at small times for particular applications of these methods.

In the present paper we address two such problems. The first is the roll-up of a semi-infinite vortex sheet with an initially parabolic circulation distribution. The second is the problem of power-law starting flow past a semi-infinite wedge with vortex separation at the wedge apex. The latter case may be regarded as the unsteady analogue of a class of slender-body flows with leading-edge separation treated by Smith (1968, 1971, 1972). Kaden (1931) first proposed the $(\text{time})^{\frac{3}{2}}$ law for the roll-up of a semi-infinite vortex sheet and obtained an asymptotic solution for the shape of the inner spiral portion. This work was extended by Moore (1975) and by Guiraud & Zeytounian (1977), who obtained higher-order elliptical corrections to Kaden's nearly circular spiral. The effect of viscosity in diffusing the vorticity on the sheet to form a rotational but essentially inviscid core and a viscous subcore has been analysed by Moore & Saffman (1973). There seems to have been no attempt to determine the detailed sheet shape numerically although Moore (1975) suggested a scheme for doing so. The appropriate similarity law for the wedge starting flow appears to have been originally discovered by Prandtl (see Smith 1966), while attempts at a solution for the flat-plate case (zero wedge angle) have been made by Anton (1939) and Wedemeyer (1961). A discrete-vortex solution for non-zero wedge angles was obtained by Rott (1956), who also derived the asymptotic form for the rolled-up spiral. The most complete numerical treatment of the problem is that due to Blendermann (1969), who obtained a family of solutions consisting for the most part of a single outer turn of the sheet from the apex and an isolated vortex representing the inner rolled-up part. Only for the case of impulsively started flow about a flat plate is enough of the sheet included to probe the asymptotic rolled-up region and the indication is of a nearly circular spiral. Finally, Fink & Soh (1974) have applied their vortex rediscretization method to the impulsive flat-plate flow and obtained good results.

In the following we apply the model consisting of a vortex sheet, a cut and an isolated vortex developed by Smith (1968) to the roll-up of a semi-infinite vortex sheet and also to the wedge starting flow. For both problems about four turns of the rolled-up sheet are included in the calculations, which takes the solutions well into the spiral region where the sheet spacing is small compared with the local radius of

curvature. Details of the numerical solutions are presented, including the self-similar vortex-sheet shapes and, for some cases, the self-similar flow streamline patterns. Comparison of some aspects of the solutions with the leading-order asymptotic solutions of Kaden (1931) and Rott (1956) are also presented and their significance is discussed.

2. The roll-up of a semi-infinite vortex sheet

2.1. *Formulation*

The roll-up of an initially plane semi-infinite vortex sheet has become known as 'Kaden's problem' (after Kaden 1931) and may be formulated as follows (see Moore 1975). An initial flow for $t < 0$ is defined as steady attached potential flow around a semi-infinite flat plate $z = x + 0i, x \leqslant 0$, with complex velocity potential

$$W = \Phi + i\Psi = -iaz^{\frac{1}{2}}, \tag{1}$$

where $z = x + iy$ is the complex-plane variable and a is a real positive constant. At $t = 0$ the rigid flat plate is removed or dissolved, leaving a semi-infinite vortex sheet with circulation $\Gamma = 2a|x|^{\frac{1}{2}}$ in $(x, 0)$ and local sheet strength $\gamma = |d\Gamma/dx| = a|x|^{-\frac{1}{2}}$. The self-induced velocity field of the sheet is infinite as $x \to 0$ and this singularity is resolved through an unsteady spiral-like roll-up of the sheet for $t > 0$, beginning at the sheet tip and subsequently entraining the whole sheet. This problem approximates the initial period of roll-up near the ends of a finite sheet with an initially elliptic circulation distribution, of the kind shed by a rectangular aerofoil moving with uniform velocity.

Adopting the formulation of Moore (1975), we describe the position of the sheet by the complex function $z_0(\Gamma, t)$, where a particular value of Γ denotes a particular constituent fluid particle (a vortex line) of the sheet. The (general) equation of motion of the two-dimensional sheet is

$$\partial \bar{z}_0(\Gamma, t)/\partial t = dW/dz \tag{2}$$

(the bar denotes the complex conjugate), where the left side is the Lagrangian velocity of a sheet fluid particle and the right side is the Eulerian complex velocity field. Equation (2) simply says that the fluid particles comprising the sheet convect with the local fluid velocity. It automatically satisfies the conditions of continuous normal velocity and pressure across the sheet. For a semi-infinite sheet we have, for a general point in the z plane,

$$\frac{dW}{dz} = \frac{1}{2\pi i}\int_0^\infty \frac{d\Gamma'}{z - z_0(\Gamma', t)}. \tag{3}$$

It is well known that the right-hand side of (3) is discontinuous across the sheet, taking different values according to the Plemelj formula

$$\frac{dW}{dz}(z_0)^{\pm} = \pm\frac{1}{2}\left(\frac{\partial z}{\partial \Gamma}\right)^{-1} + \frac{1}{2\pi i}\mathrm{P}\int_0^\infty \frac{d\Gamma'}{z_0 - z_0(\Gamma', t)} \tag{4}$$

as a point $z_0(\Gamma, t)$ on the sheet is approached from the $\pm$ side. The integral in (4) is the Cauchy principal value integral (see Muskelishvili 1946, p. 26) and is equal to the mean of the limiting complex velocities on the $\pm$ sides of $z_0(\Gamma, t)$. Since this integral

may be shown to be equal to the local self-inductive velocity of the vortex sheet, substitution into (2) leads to an initial-value problem for $z_0(\Gamma, t)$ given by

$$\frac{\partial \bar{z}_0}{\partial t} = \frac{1}{2\pi i} \mathrm{P} \int_0^\infty \frac{d\Gamma'}{z_0 - z_0(\Gamma', t)} \tag{5}$$

with initial condition

$$z_0(\Gamma, 0) = -\tfrac{1}{4}\Gamma^2/a^2. \tag{6}$$

A dimensional analysis of the above problem suggests the existence of a similarity solution of the form

$$z_0(\Gamma, t) = (at)^{\frac{2}{3}} \omega(\lambda), \tag{7}$$

where $\omega(\lambda) = \xi(\lambda) + i\eta(\lambda)$ is the non-dimensional self-similar shape function for the sheet, a function of the non-dimensional circulation parameter

$$\lambda = \Gamma/(a^{\frac{1}{3}} t^{\frac{1}{3}}). \tag{8}$$

Substitution of (7) and (8) into (5) leads to an integro-differential equation for $\omega(\lambda)$:

$$\tfrac{1}{3}(2\bar{\omega} - \lambda\, d\bar{\omega}/d\lambda) = d\Omega/d\omega, \tag{9a}$$

where the non-dimensional complex velocity is

$$\frac{d\Omega}{d\bar{\omega}} = \frac{1}{2\pi i} \mathrm{P} \int_0^\infty \frac{d\lambda'}{\omega(\lambda) - \omega(\lambda')}. \tag{9b}$$

Equations (6)–(8) show that $\omega(\lambda)$ must satisfy

$$\omega(\lambda) \sim -\tfrac{1}{4}\lambda^2 \quad \text{as} \quad \lambda \to \infty. \tag{10}$$

Equations (7) and (8) show that W is related to the non-dimensional complex velocity potential $\Omega = \phi + i\psi$ by

$$W(z, t) = a^{\frac{1}{3}} t^{\frac{2}{3}} \Omega[z/(at)^{\frac{2}{3}}]. \tag{11}$$

2.2. *Numerical solution of the integro-differential equation*

An approximate numerical solution to (9) is to be obtained by applying the model consisting of a vortex sheet, a cut and an isolated vortex developed by Smith (1968) for the treatment of leading-edge separation from a slender delta wing. The adaptation of the model to the present problem is as follows. The vortex sheet in the ω plane is divided into three sections.

(i) A section described by (10) and defined by $\infty > \lambda \geqslant \lambda_0 > 0$, thus extending from $\omega = -\infty + 0i$ to $\omega_0 = -\tfrac{1}{4}\lambda_0^2 + 0i$. This section is to be regarded as an undisturbed straight portion of the sheet remote from the spiral predicted by asymptotic solutions.

(ii) An intermediate section defined by $\lambda_0 > \lambda \geqslant \lambda_N > 0$ divided into N straight subsections $\lambda_{k-1} \geqslant \lambda > \lambda_k$ with end points ω_{k-1} and ω_k ($k = 1, \ldots, N$). The value of λ_0 chosen must be sufficiently large that the solution obtained approximates (10) for small values of $k = 1, 2, \ldots$, and this can be verified only *a posteriori*. The value of λ_N will be such that a substantial portion of the rolled-up sheet is included in this section.

(iii) An inner part $\lambda_N > \lambda > 0$ over which we may regard the sheet as approximated by the tightly wound asymptotic spiral. For a point on the sheet $\lambda > \lambda_N$, the contribution to the complex velocity due to this part may be approximated by that due to an isolated vortex of strength λ_N placed at the 'centre of circulation' in $(0, \lambda_N)$,

which we denote by $\omega_v = \omega_{N+1}$ (for a justification see Smith 1966). To define Ω uniquely in this region, ω_{N+1} is joined to ω_N by a cut of arbitrary shape in the ω plane which, together with the vortex sheet, defines an entire cut for a single-valued Ω. Note that the cut (ω_N, ω_{N+1}) itself plays no part in the actual calculation since $d\Omega/d\omega$ is single valued in this region and Ω itself is not required.

With the above representation of the sheet, for a point on the sheet $\lambda > \lambda_N$, (9*b*) may be approximated as

$$\frac{d\Omega}{d\omega} = F(\omega) + \frac{1}{2\pi i}\sum_{j=1}^{N}\int_{\lambda_{j-1}}^{\lambda_j}\frac{d\lambda'}{\omega-\omega(\lambda')} + \frac{\lambda_N}{2\pi i(\omega-\omega_{N+1})}, \tag{12a}$$

where

$$F(\omega) = -\frac{1}{2\pi\omega^{\frac{1}{2}}}\left[i\pi - \log\left(\frac{\omega^{\frac{1}{2}}-\frac{1}{2}i\lambda_0}{\omega^{\frac{1}{2}}+\frac{1}{2}i\lambda_0}\right)\right] \tag{12b}$$

and where the three terms in (12*a*) correspond respectively to the contributions from the three parts of the sheet.

We satisfy a finite-difference form of (9) at the midpoints

$$\omega_{k-1,k} = \tfrac{1}{2}(\omega_{k-1}+\omega_k), \quad \lambda_{k-1,k} = \tfrac{1}{2}(\lambda_{k-1}+\lambda_k) \quad (k = 1, \ldots, N) \tag{13}$$

of each of the N straight elements forming section (ii) of the sheet. The $d\bar{\omega}/d\lambda$ on the left-hand side of (9*a*) is replaced by a two-point differentiation rule while (9*b*) is approximated by (12) with each of the N integrals evaluated using the trapezoidal rule, ignoring the Cauchy principal value singularity for $j = k$. For the contribution of the kth element at $\omega_{k-1,k}$, this may be shown to give the same result, namely zero, as an evaluation in which a linear variation of ω with λ is assumed in $(\lambda_k, \lambda_{k-1})$ with proper treatment of the Cauchy principal value. Note, however, that use of the trapezoidal rule for the velocity induced by a sheet element at points on or off the element which are near but not at the midpoint can lead to serious inaccuracies owing to the neglect of logarithmic terms which vanish at the midpoint (see Fink & Soh 1974; appendix B herein). The finite-difference form of (9) then becomes

$$\tfrac{1}{2}[\bar{\omega}_k(1-C_{k-1,k})+\bar{\omega}_{k-1}(1+C_{k-1,k})] + \frac{i}{2\pi}\sum_{j=0}^{N+1}\frac{A_j}{\omega_{k-1,k}-\omega_j} - F(\omega_{k-1,k}) = 0 \quad (k = 1, \ldots, N), \tag{14}$$

where

$$C_{k-1,k} = \tfrac{1}{2}(\lambda_{k-1}+\lambda_k)/(\lambda_{k-1}-\lambda_k),$$

$$A_0 = \tfrac{1}{2}\lambda_1, \quad A_j = \tfrac{1}{2}(\lambda_{j-1}-\lambda_{j+1}) \quad (j = 1, \ldots, N-1),$$

$$A_N = \tfrac{1}{2}(\lambda_{N-1}-\lambda_N), \quad A_{N+1} = \lambda_N$$

and where (14) represent $2N$ real equations.

Since there is no hope of satisfying (9) element by element for $\lambda < \lambda_N$, we integrate (9*a*) over $(0, \lambda_N)$ to obtain

$$\int_0^{\lambda_N}\bar{\omega}\,d\lambda - \tfrac{1}{3}\lambda_N\bar{\omega}_N = \int_0^{\lambda_N}\left(\frac{d\Omega}{d\omega}\right)d\lambda. \tag{15}$$

By making the approximations

$$\int_0^{\lambda_N}\bar{\omega}\,d\lambda \simeq \lambda_N\bar{\omega}_{N+1}, \quad \int_0^{\lambda_N}\left(\frac{d\Omega}{d\omega}\right)d\lambda \simeq \lambda_N\left(\frac{d\Omega}{d\omega}\right)_{\omega_{N+1}}, \tag{16}$$

substituting into (15) and using (12), we obtain the following averaged form of (9) in $(0, \lambda_N)$:

$$\overline{\omega}_{N+1} - \tfrac{1}{3}\overline{\omega}_N + \frac{i}{2\pi}\sum_{j=0}^{N}\frac{A_j}{\omega_{N+1}-\omega_j} - F(\omega_{N+1}) = 0. \tag{17}$$

Equation (17) is equivalent to the so-called 'zero-force' condition used by Smith (1968) over the inner part of the sheet for the slender-body leading-edge separation problem.

For fixed λ_j $(j = 1, \ldots, N)$, (14) and (17) may be regarded as $2(N+1)$ nonlinear equations for the $2(N+1)$ unknowns ξ_j and η_j $(j = 1, \ldots, N+1)$. Instead of this scheme, however, we adopt a more convenient one through the transformation

$$\lambda_j = \mu_j \lambda_N \quad (j = 1, \ldots, N-1), \tag{18a}$$

$$\omega_j = \omega_{N+1} - \rho_j \exp\left[i(\chi_j + \chi_v)\right] \quad (j = 1, \ldots, N), \tag{18b}$$

$$\omega_{N+1} = \omega_0 + \rho_v \exp\left(i\chi_v\right), \tag{18c}$$

where $\rho_j = |\omega_j - \omega_{N+1}|$ and the χ_j are the anticlockwise polar angles about ω_{N+1} of the ω_j, measured from the datum line (ω_0, ω_{N+1}). Substituting (18) into (14) and (17) and regarding the χ_j as constants, i.e. assuming a fixed angular separation between the ω_j, we obtain a set of $2N+2$ equations which we write as

$$f_q(\mathbf{X}) = 0 \quad (q = 1, \ldots, 2N+2) \tag{19}$$

for the $2N+2$ unknown components of the $(2N+2)$-fold

$$\mathbf{X} = (\rho_v, \rho_1, \rho_2, \ldots, \rho_N, \mu_1, \mu_2, \ldots, \mu_{N-1}, \lambda_N, \chi_v). \tag{20}$$

For the present problem and for the starting-flow problem a solution to (19) was obtained using a Newton–Raphson scheme employed by the author (see Pullin 1975) for the treatment of the leading-edge separation problem. All solutions, say $\mathbf{X}^*$, reported here satisfied the condition

$$\sum_{q=1}^{2N+2} |f_q(\mathbf{X}^*)| = o(10^{-8}),$$

which is regarded as giving a sufficiently accurate solution of the algebraic equations if not the corresponding integro-differential equation.

2.3. *Numerical results*

The solution to Kaden's problem presented here was obtained with $N = 97$, this value being the largest that could be adopted within the limits of computer storage. The angular separation $\chi_j - \chi_{j-1}$ of points on the sheet was chosen as about 20°, i.e. about 18 points per turn of the sheet. Since the solution method is iterative, an initial approximation was required. This was obtained in the first instance for $N = 40$ by guessing a value of ω_{N+1} and patching a sheet shape given by Kaden's (1931) asymptotic solution [see (21)] onto a length of straight undisturbed sheet given by (10). The solution for $N = 97$ was then obtained by extending the $N = 40$ solution by again using the asymptotic solution but with improved values of the arbitrary constants.

The solution points representing the self-similar sheet shape shown in figure 1 correspond to $\lambda_0 = 3{\cdot}6$ and $\omega_0 = -3{\cdot}24 + 0i$. That the numerical solution indeed

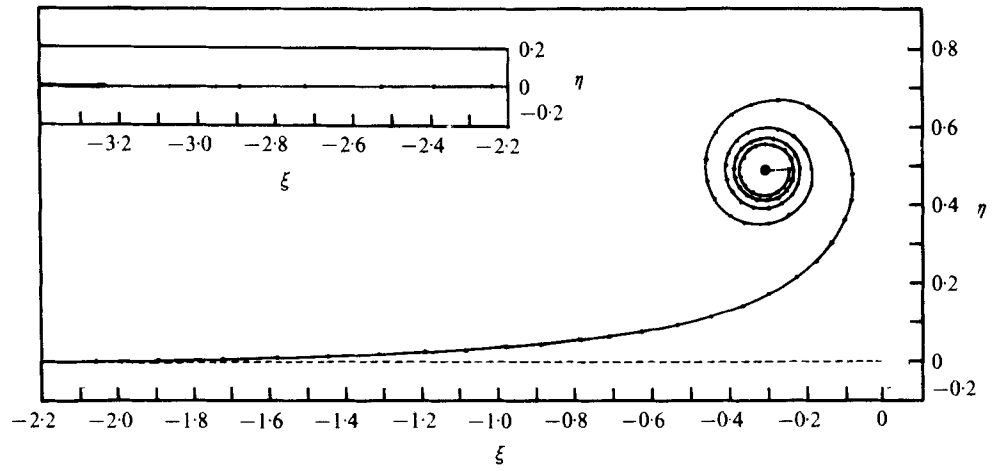

FIGURE 1. —·—, self-similar vortex-sheet shape in the $\omega = \xi + i\eta$ plane, $\xi > -2{\cdot}2$, $N = 97$. Inset: solution continued for $\xi < -2{\cdot}2$; ——, fixed sheet, $-\infty < \xi < -3{\cdot}24$.

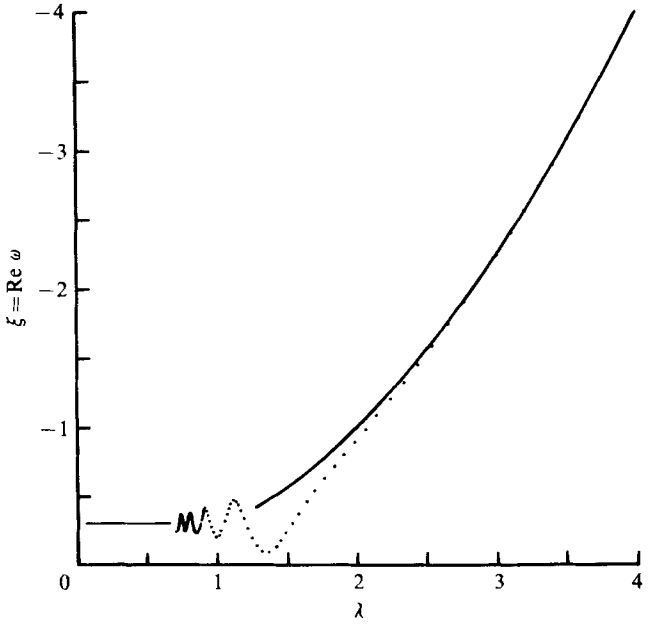

FIGURE 2. Numerical and large λ asymptotic solution. ——, asymptotic; ·····, numerical, $N = 97$; ——, isolated vortex position.

asymptotes to the large-λ solution is clearly demonstrated in figure 2, where the first seven or eight calculated points are indistinguishable from the curve representing (10). At the other end of the sheet, if, following Moore (1974), the roll-up process is reckoned to begin where the sheet is first vertical ($j = 29$), then about four turns of the spiral are included in the solution. Here the value of λ is $\lambda_{29} = 1{\cdot}342$ compared with $\lambda_{97} = 0{\cdot}7123$. Thus at any instant in the unsteady roll-up process, the amount of circulation contained in the spiral region is $\Gamma_{sp} \simeq 1{\cdot}34a^{\frac{4}{3}}t^{\frac{1}{3}}$, and about 50% of this circulation resides on the outer four spiral turns.

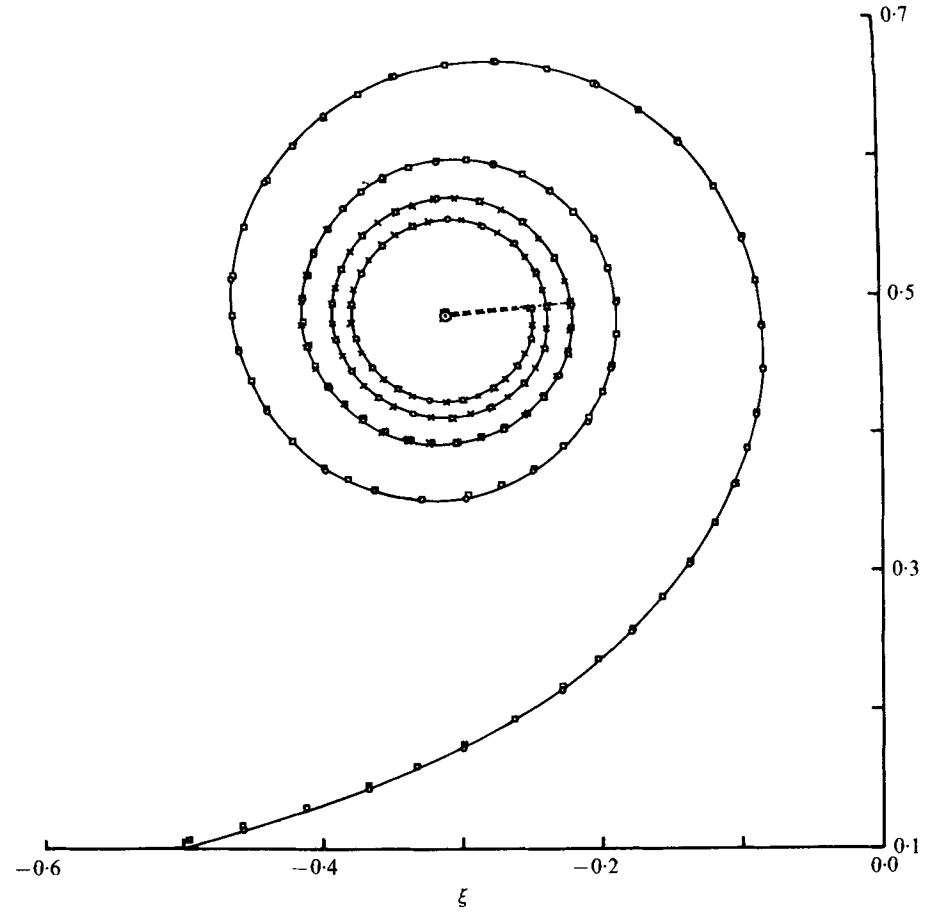

FIGURE 3. Inner part of sheet in the $\omega = \xi + i\eta$ plane, showing effect of step size. ○, type A solution, $N = 97$; □, type B solution, $M = 110$, $N = 94$; ×, type B solution, $M = 142$, $N = 94$.

Owing to the complexity of (9), an analysis of errors incurred in the calculations is rather difficult. The most likely source, however, is the use of the trapezoidal rule for the velocity-inducing effect of the segmented part of the sheet. For a particular segment the major part of this error will come from the immediately adjacent sheet segments. For the overall solution, the cumulative error will depend on the relative magnitude of local and far-field contributions to the local velocity, and may be expected to depend on the ratio $\delta s/\delta\rho$ of arc-length step size along the sheet to sheet spacing, particularly in the spiral region, where the $N = 97$ solution indicates a tightly wound sheet with a ratio of sheet spacing to radius $\delta\rho/\rho \ll 1$. In addition to this solution, referred to as 'type A' in figure 3, two additional, 'type B' solutions were obtained to estimate the effects of step size. These differ from the type A solutions in the following sense. For the type A solution, the solution in $\infty > \lambda \geqslant \lambda_0$ is assumed to be given [by (10)] and that in $\lambda_0 > \lambda > 0$ is obtained as described in § 2.2. For the type B solution, the solution in $\infty > \lambda \geqslant \lambda_{M-N}$ is assumed to be given by (10) in $\infty > \lambda > \lambda_0$ and by $M-N$ points ω_j ($j = 1, \ldots, M-N$, with $M > N$) in $\lambda_0 > \lambda > \lambda_{M-N}$, obtained from the known type A solution. The solution in $\lambda_{M-N} > \lambda > 0$ is then obtained

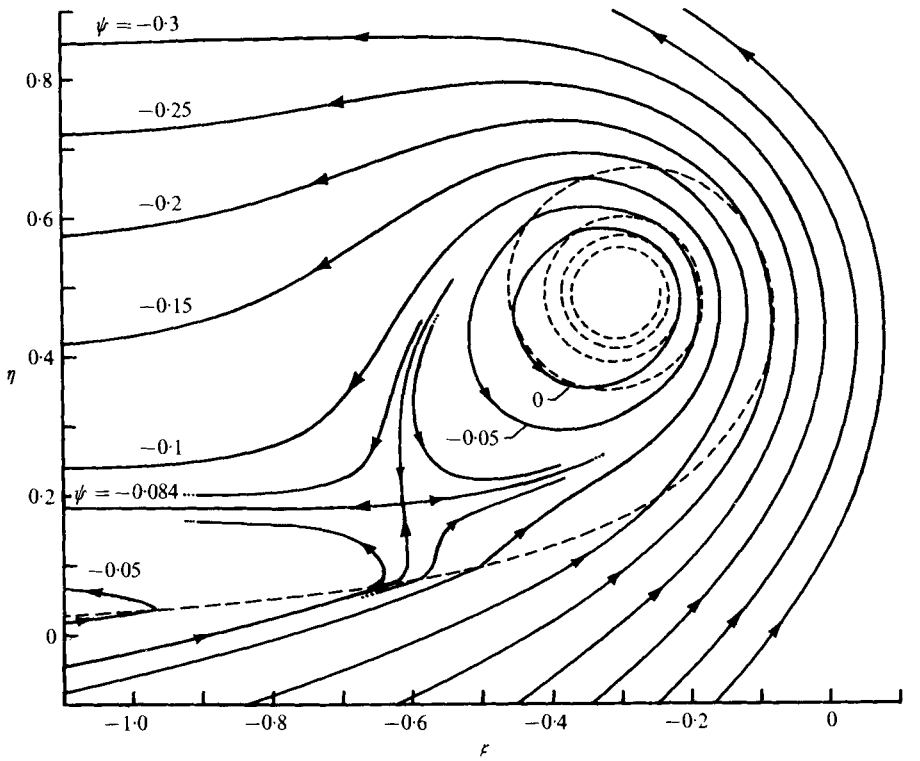

FIGURE 4. Instantaneous streamlines in the ω plane for Kaden's problem. ——, streamlines; – – –, vortex sheet.

exactly as for the type A solution but now with $2(N+1)$ unknowns given by ω_j $(j = M-N+1, M+1)$. This technique allowed approximate halving of the step size over tightly wound portions of the sheet which were felt to be probably most sensitive to step size, while still handling a manageable number of unknowns. Figure 3 indicates that the effect of step size, as so tested, on the sheet shape is small compared with $\delta\rho$. This is not entirely conclusive however, since the far-field errors due to the trapezoidal rule for a single segment are of order $(\delta s/R)^2$, where R is the distance to the segment's midpoint and, even for the $M = 142$, $N = 94$ solution, we still have $\delta s/\delta\rho = O(1)$. Further discussion of this question is given in appendix B, where it is argued that, owing to error cancellation, errors remain small even for $\delta s/\delta\rho = O(1)$.

Since the position $\omega_{98} = -0{\cdot}308 + 0{\cdot}489i$ of the isolated vortex is the present estimate of the spiral sheet's centre, it follows from (7) that the trajectory of this point is $z(0,t) = (at)^{\frac{2}{3}}(-0{\cdot}308 + 0{\cdot}489i)$. In terms of the critical points of the velocity field (see Perry & Fairlie 1974), $z(0, t)$ will appear as a moving centre as indicated in figure 4, where instantaneous or self-similar streamlines $\psi = \operatorname{Im}\Omega$ are shown. From (11) it follows that the actual streamlines expand with the vortex sheet in a wavelike fashion. The other major feature of the flow field is a moving saddle point $\omega = -0{\cdot}615 + 0{\cdot}190i$ for which $\psi = -0{\cdot}084$. For a symmetrical vortex sheet with an elliptical circulation distribution, the singular points on each half of the z plane would consist of a centre and a saddle point corresponding to those for the semi-infinite sheet together with another centre lying on the vortex sheet.

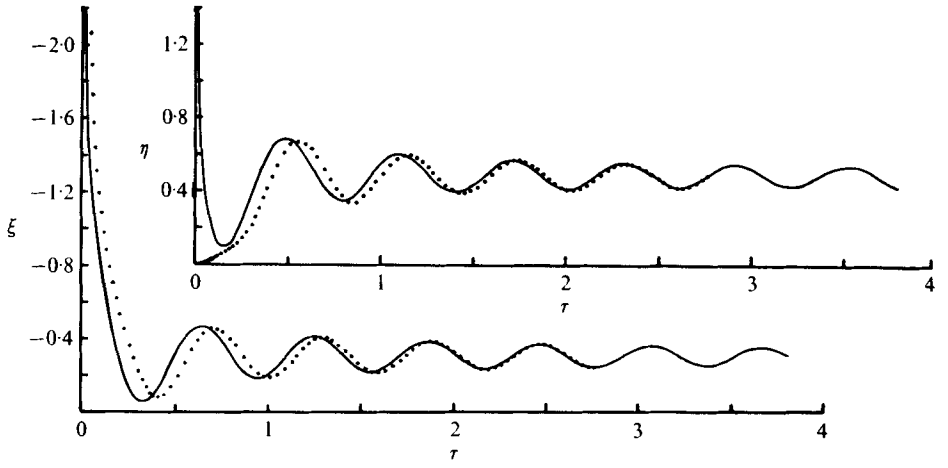

FIGURE 5. Comparison of numerical and asymptotic solution to Kaden's problem. ·····, present numerical; ——, asymptotic (Kaden 1931).

2.4. *Comparison with asymptotic solution*

Kaden's (1931) original asymptotic solution may be written as

$$\omega - \omega_v = \alpha \tau^{-\frac{5}{3}} \exp[i(\tau/2\pi\alpha^2 + \epsilon)], \tag{21}$$

where $\tau = \lambda^{-3}$ and α and ϵ are arbitrary constants. This solution represents a tightly wound spiral with nearly circular turns, and may be shown to be dominated by circulation on the sheet between a point $\omega(\lambda)$ and the spiral centre. Moore (1975) obtains a large-τ asymptotic solution of (9) as a second-order term in a series for which (21) represents the leading term while Guiraud & Zeytounian (1977) obtain further terms using a rather different approach. These higher-order terms represent ellipticity in the sheet shape, which Moore (1975) interprets as the straining effect on the rolled-up spiral of the remote, unrolled portions of the sheet. Consequently, if one takes an asymptotic solution of any desired order larger than the first, then the various constants appearing, including α and ϵ, can be determined only from the flow field as a whole, i.e. from the complete solution for $\omega(\lambda)$. The labour involved in determining the constants to second order from Moore's (1975) solution is considerable however, and since figure 3 indicates that the effects of ellipticity are not large (i.e. the turns appear to be approximately circular with monotonically decreasing radius) we shall restrict ourselves to comparison with the first-order solution (21). In this case an approximation to α and ϵ may be obtained by patching the numerical and asymptotic solutions at some point along the sheet. We arbitrarily choose $j = 96$ (avoiding the last point $j = 97$ because of possible end effects), which yields $\alpha = 0{\cdot}124$ and $-\pi < \epsilon < \pi$, $\epsilon = 2{\cdot}69$. Of course this procedure is reasonable only if the α and ϵ thus obtained do not depend too strongly on j. If the solutions are patched for $j = 73$, we obtain $\alpha = 0{\cdot}125$ and $\epsilon = 2{\cdot}75$, while for $j = 50$, $\alpha = 0{\cdot}122$ and $\epsilon = 1{\cdot}83$. It is significant that these values of α differ appreciably from the value $\alpha = \frac{1}{6}$ obtained from an approximate argument due to Betz and reproduced by Moore & Saffman (1973; see also Moore 1975). Figure 5 compares the numerical and asymptotic solutions for the real and imaginary parts of $\omega(\tau)$ with (21) for $\alpha = 0{\cdot}124$ and $\epsilon = 2{\cdot}69$. The qualitative features

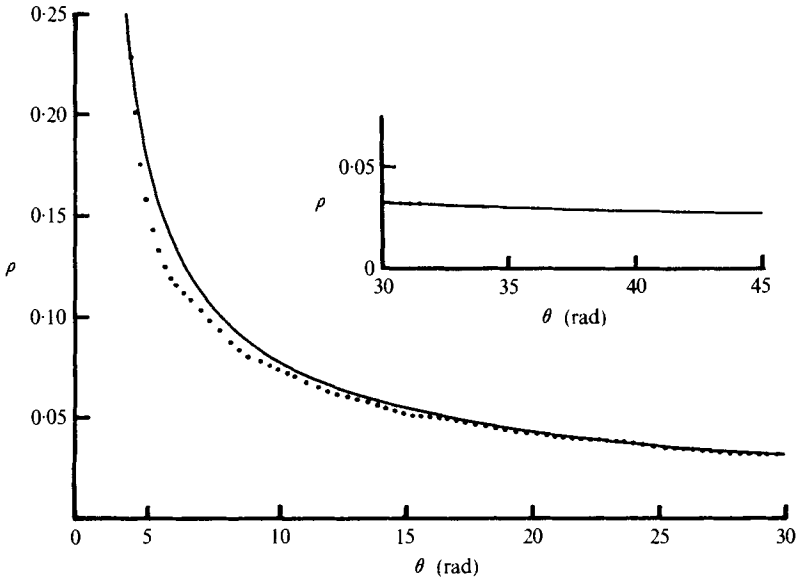

FIGURE 6. Vortex-sheet ρ, θ relationship. · · · · ·, present numerical; ——, asymptotic (Kaden 1931).

of the solutions are quite similar for the whole range of τ shown, the relationship between period and amplitude in (21) being approximately preserved in the present solution.

The clearest indication of possible ellipticity in the sheet shape may be obtained from its ρ, θ relationship, where ρ and θ are polar co-ordinates of a point on the sheet, with $\rho = 0$ at the spiral centre. Putting $\theta = \tau/2\pi\alpha^2 + \epsilon$ in (21) and eliminating τ yields

$$\rho = (2\pi)^{-\frac{2}{3}}\alpha^{-\frac{1}{3}}/(\theta - \epsilon)^{\frac{2}{3}}, \tag{22}$$

which is Kaden's well-known result for the sheet shape. This may be compared with the numerical solution by choosing the origin of θ such that $\theta_{96} = \tau_{96}/2\pi\alpha^2 + \epsilon$. Figure 6 shows good agreement, and clearly indicates that elliptical distortions in the sheet shape are small after the first few turns.

Some insight into the sheet behaviour during roll-up may be obtained by following the motion, from $t = 0$, of a typical fluid particle on the sheet. Noting that a constant value $\Gamma = \Gamma_0$ marks a material fluid particle, Moore & Saffmann (1973) showed from the first-order solution that a particle with initial position $x_0 = -\Gamma_0^2/4a^2$ will move, for large t, in a circular orbit (to first order) of radius $r_0 = \alpha\Gamma_0^2/a^2$ around the sheet centre with azimuthal velocity $V_\theta = a^2/(2\pi\alpha\Gamma_0)$. In addition they showed that the distance between successive sheet turns decreases as $\delta r \simeq 4\pi r_0^{\frac{5}{2}}/(3at)$. The significance of these results may be seen by considering the local sheet strength

$$\gamma(\Gamma, t) = \left|\left(\frac{\partial z}{\partial \Gamma}\right)_t\right|^{-1}, \tag{23}$$

which is equal to the magnitude of the local tangential velocity discontinuity across the sheet. From (6) it follows that if a sheet particle has $\Gamma = \Gamma_0$ then $\gamma(\Gamma_0, 0) = 2a^2/\Gamma_0$, while from (6) and (7) we obtain

$$\gamma(\tau)/\gamma(\tau = 0) = \tfrac{1}{6}\tau^{-\frac{5}{3}}|d\omega/d\tau|^{-1}, \tag{24}$$

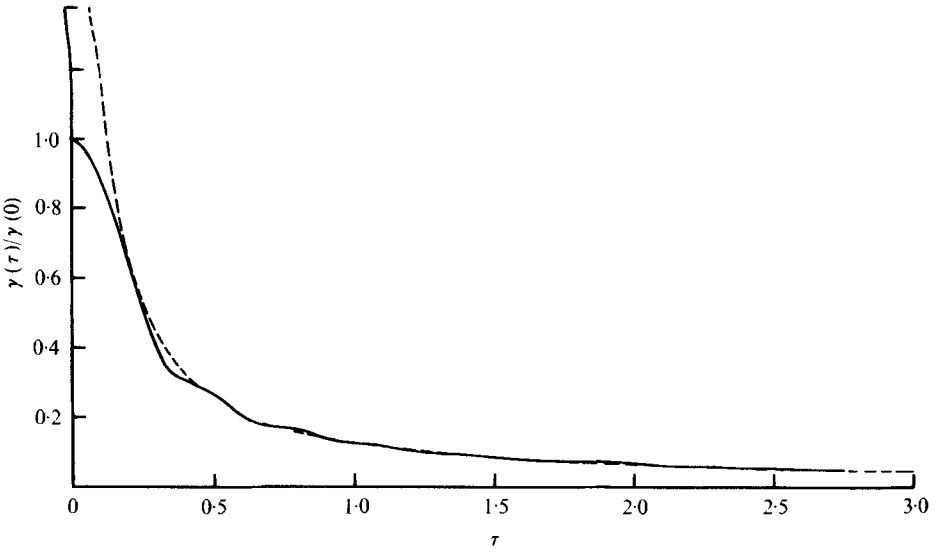

FIGURE 7. Variation of vortex-sheet strength with dimensionless time following a fluid particle. ——, present calculation; – – –, asymptotic (Kaden 1931).

where $\tau = a^4 t/\Gamma_0^3$ is the non-dimensionalized time as in (21). For large τ, (21) then gives to leading order

$$\gamma(\tau)/\gamma(0) = \tfrac{1}{3}\pi\alpha\tau^{-1}. \tag{25}$$

The comparison of (25) with the present numerical results in figure 7 shows excellent agreement. The decrease in γ as $\gamma \sim \Gamma_0^2 t^{-1}$ corresponds to a local stretching of the sheet at a constant radius of curvature r_0 as we follow the fluid particle, the result of which is the decrease in spacing of successive turns as t^{-1} indicated earlier.

3. Starting flow past an infinite wedge

3.1. *Formulation*

We now turn to the problem of inviscid starting flow past an infinite wedge. Consider two-dimensional flow, starting from rest at $t = 0$, of an incompressible fluid past a stationary boundary with a corner of angle $\beta\pi$ ($1 > \beta \geqslant 0$). As the flow accelerates, the boundary layer which forms on the windward edge of the corner will be unable to negotiate the sharp apex and will separate, forming a free shear layer which rolls up into a coherent spiral-like structure illustrated in the well-known flow visualizations of Prandtl & Tietjens (see Batchelor 1970, figure 6.7.2). Near the salient edge, the boundary layer may be expected to grow as $(\nu t)^{\frac{1}{2}}$, where ν is the kinematic viscosity, while, as will be seen, the minimum growth rate of the spatial scale of the separated structure as a whole is as $t^{\frac{3}{2}}$. Hence after a small initial period δt of slow viscous flow, it is reasonable to model the separated shear layer by a vortex sheet expanding from the salient edge into an otherwise irrotational flow.

We therefore consider a potential flow, starting from rest, for which the overall complex potential for attached flow is of the form

$$W(z,t) = At^m F(z), \tag{26}$$

where $z = x+iy$ is the complex variable in the physical plane, $m \geqslant 0$ is the time exponent, A is a constant and $F(z)$ satisfies the appropriate boundary conditions in the z plane. Near the salient edge, which we take as the origin in the z plane, the leading term in the expansion of $W(z,t)$ for small z is of the form

$$W = -iat^m z^n, \tag{27}$$

where $n = 1/(2-\beta)$, a is a real positive constant and where (27) represents attached flow past an infinite wedge of angle $\beta\pi$ positioned in the z plane as shown in figures 9(*a*)–(*c*). The singularity of the form z^{n-1} in the complex velocity for $z \to 0$ in (27) is removed by introduction of a vortex sheet representing the separated shear layer. We again use a Lagrangian description $z_0(\Gamma,t)$ of the vortex sheet, where Γ is the discontinuity in $\Phi = R(W)$ across the sheet at $z_0(\Gamma,t)$ or, equivalently, the total circulation lying on the sheet between z_0 and the rolled-up sheet tip. For t less than some interval Δt (estimates of both Δt and δt can be readily obtained), the evolution of the sheet will be dominated by the attached flow (27), i.e. the sheet will initially see the wedge as infinite. By introducing the conformal mapping

$$z^* = z^n, \tag{28}$$

which maps the flow region $\pi(1-\frac{1}{2}\beta) \geqslant \arg z \geqslant -\pi(1-\frac{1}{2}\beta)$ into the right-hand half of the z^* plane, the complex velocity at a point in the z plane may be readily constructed, and equation (2) for the motion of $z_0(\Gamma,t)$ becomes

$$\overline{\frac{\partial z_0(\Gamma,t)}{\partial t}} = nz_0^{n-1}\left\{-iat^m - \frac{1}{2\pi i}\,\mathrm{P}\int_{\Gamma_s(t)}^{0}\left[\frac{1}{z_0^n(\Gamma,t)-z_0^n(\Gamma',t)} - \frac{1}{z_0^n(\Gamma,t)+\overline{z_0^n(\Gamma',t)}}\right]d\Gamma'\right\}, \tag{29}$$

where the integral term represents the contribution to the complex velocity at $z_0(\Gamma,t)$ of the line distributions of circulation representing the vortex sheet and its image in the wedge. The total circulation shed from the edge at time t is $\Gamma_s(t)$ and is determined by requiring that dW/dz be finite as $z \to 0$. Since the z_0^{n-1} factor on the right-hand side of (29) is singular as $z_0 \to 0$, this requires that

$$-iat^m + \frac{1}{2\pi i}\int_{\Gamma_s(t)}^{0}[\bar{z}_0^n(\Gamma',t) + \overline{z_0^n(\Gamma',t)}]\,d\Gamma' = 0, \tag{30}$$

which is the well-known Kutta condition for the present problem.

No natural length or velocity scale is provided by the boundary conditions on the attached flow given by (27). Dimensional analysis then suggests the existence of a similarity solution to (29) and (30), which we write as

$$z_0(\Gamma,t) = Ca^{1/(2-n)}t^{(1+m)/(2-n)}\omega(\lambda). \tag{31}$$

Here $\omega(\lambda) = \xi(\lambda)+i\eta(\lambda)$ is the non-dimensional self-similar shape function for the sheet, a function of the dimensionless combination

$$\lambda = 1 - \frac{\Gamma}{C^n a^{2/(2-n)}t^{2(1+m)/(2-n)-1}J} \tag{32}$$

of Γ and t, where J is a constant to be determined. The scaling constant

$$C = \left[\frac{(2-n)(1-n)}{1+m}\right]^{1/(2-n)} \tag{33}$$

can be extracted from Rott's (1956) analytical discrete-vortex solution and is introduced so as to keep $\omega(\lambda)$ finite in the limits $m \to \infty$ and possibly $n \to 1$. Note that the minimum value of $\frac{2}{3}$ for the time exponent in (31) occurs for $m = 0$ and $n = \frac{1}{2}$. The parameter λ takes the value $\lambda = 0$ at the wedge apex and the value $\lambda = 1$ at the tip or centre of the rolled-up sheet. It then follows from (32) that $\Gamma_s(t)$ is given by

$$\Gamma_s(t) = C^n a^{2/(2-n)} t^{2(1+m)/(2-n)-1} J. \tag{34}$$

Equations (31), (32) and (34) are the similarity laws for the wedge problem discovered by Prandtl, Rott (1956) and other workers.

Substituting (31), (32) and (34) into (29) yields the following complex integro-differential equation for $\omega = \omega(\lambda)$ $(0 \leqslant \lambda \leqslant 1)$:

$$(1-n)\left[\bar{\omega} + Q(1-\lambda)\frac{d\bar{\omega}}{d\lambda}\right] = \frac{d\Omega}{d\omega}, \tag{35a}$$

where

$$\frac{d\Omega}{d\omega} = n\omega^{n-1}\left\{-i + \frac{J}{2\pi i}\mathrm{P}\int_0^1 \left[\frac{1}{\omega^n - \omega^n(\lambda')} - \frac{1}{\omega^n + \overline{\omega^n(\lambda')}}\right] d\lambda'\right\} \tag{35b}$$

with $Q = 2-(2-n)/(1+m)$. Substituting the same equations into (30) leads to a single real (by symmetry) constraint on $\omega(\lambda)$ and J which is sufficient to determine J:

$$1 - \frac{J}{2\pi}\int_0^1 [\omega^{-n}(\lambda') + \overline{\omega^{-n}(\lambda')}]\, d\lambda' = 0. \tag{36}$$

From (31) and (32) it follows that W is of the form

$$W(z,t) = C^n a^{2/(2-n)} t^{2(1+m)/(2-n)-1} \Omega[z/Ca^{1/(2-n)} t^{(1+m)/(2-n)})], \tag{37}$$

where Ω is the non-dimensional complex potential. The behaviour of the solution to (35) and (36) near the wedge apex $(\lambda \to 0)$ is discussed briefly in appendix A while Rott's (1956) solution for the asymptotic spiral $(\lambda \to 1)$ is considered in § 3.4.

3.2. *Numerical solution*

For intermediate λ a numerical solution to (35) and (36) for $\omega(\lambda)$ and J was obtained by the method described in § 2.2. Here, however,we are dealing with finite rather than infinite vortex sheets. Hence for numerical purposes the sheet is divided into only two sections.

(i) A segmented section $\lambda_N \geqslant \lambda > 0$ divided into N straight subsections $\lambda_k \geqslant \lambda > \lambda_{k-1}$ with end points ω_{k-1} and ω_k $(k = 1, \ldots, N)$.

(ii) An inner part $1 > \lambda > \lambda_N$ for which the circulation $J(1-\lambda_N)$ is lumped into an isolated vortex at ω_v joined to ω_N by a cut in the ω plane.

Since the finite-difference forms of (35) and of the integrated equation in $(\lambda_N, 1)$ (zero-force condition) are then essentially similar to (14) and (17), with added complications due to solid boundaries and an image vortex sheet, we do not give them here. Equation (36), for which the integrand has an integrable singularity at $\lambda = 0$, is an extra condition for the present problem. For $\beta > 0$, the contribution to the integral in (36) from the first segment $(0, \lambda_1)$ adjoining the wedge apex was evaluated using (54) (see appendix A) while, for $\beta = 0$, (48) was used with K_1 and K_2 expressed in terms of ω_1 and λ_1. Using transformations similar to (18) with ω_0 replaced by

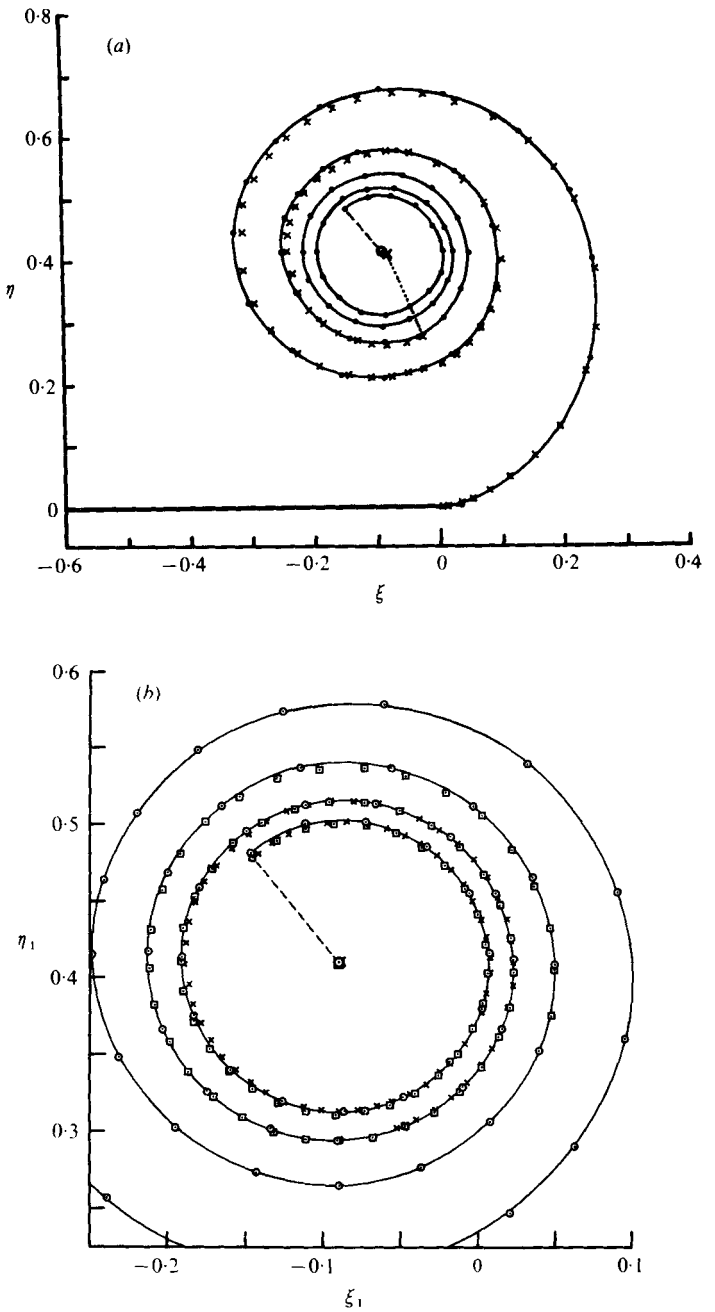

FIGURE 8. (*a*) Sheet shape in the $\omega = \eta + i\xi$ plane for $\beta = 0$, $m = 0$; ○, $N = 75$; ×, $N = 72$. (*b*) Inner part of sheet for semi-infinite flat plate in the $\omega = \eta + i\xi$ plane, showing effect of step size, for $\beta = 0$, $m = 0$. ⊙, type A solution, $N = 75$; □, type B solution, $M = 114$, $N = 75$; ×, type B solution, $M = 140$, $N = 75$.

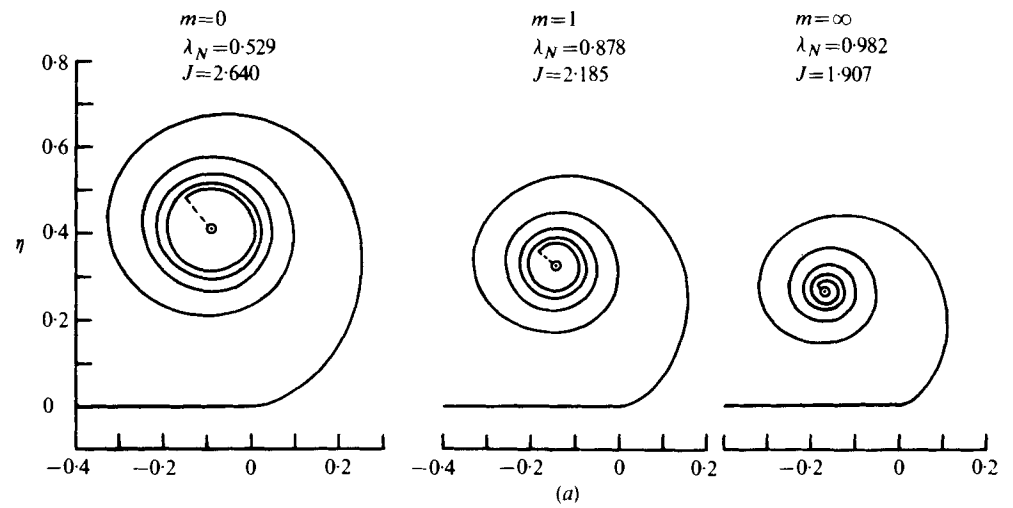

FIGURES 9 (*a*, *b*). For legend see p. 418.

$\omega_0 = 0 + 0i$, we finally obtain a set of $2N+3$ nonlinear equations for the $(2N+3)$-fold

$$\mathbf{X} = (\rho_1, \rho_2, \rho_3, \ldots, \rho_N, \rho_v, \chi_v, \mu_1, \mu_2, \ldots, \mu_{N-1}, \lambda_N, J), \tag{38}$$

where $\rho_j = |\omega_v - \omega_j|$ $(j = 1, \ldots, N)$, $\omega_v = \rho_v \exp(i\chi_v)$ and $\mu_j = \lambda_j/\lambda_N$ $(j = 1, \ldots, N-1)$. These equations were solved for a range of time exponents and wedge angles using the Newton–Raphson scheme referred to in § 2.2.

3.3. *Numerical results*

Solutions to the finite-difference equations were obtained with $N = 75$. The typical angular separation of points on the sheet was about 20°–25° except very near the apex, where the step size was gradually reduced to about 0·1° over the segment

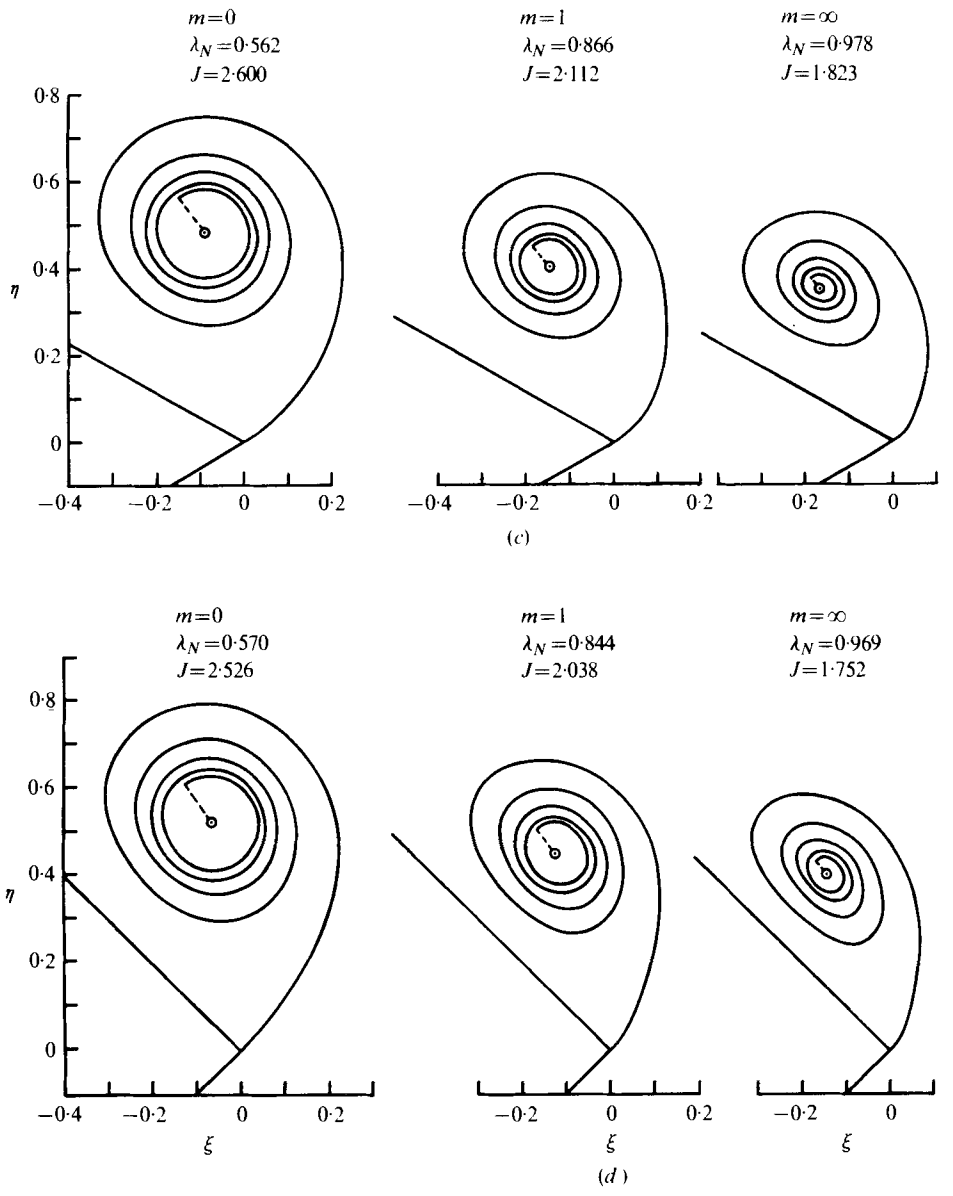

FIGURES 9(*c*, *d*). For legend see p. 418.

adjoining the wedge apex. The solutions discussed here were obtained for $m = 0$, 0·25, 0·5, 1·0, 2·0, 5·0 and ∞ and for values of β ranging from zero up to the maximum value for which solutions could be found. An initial approximation for $m = 0$ and $\beta = 0$ was obtained by using a combination of Rott's (1956) discrete-vortex solution [see (39)] and his asymptotic large λ solution [see (40)]. Additional solutions were then obtained by varying β and m, using the last found solution as an initial approximation for the next pair (m, β).

Although we should expect solutions to exhibit a sensitivity to step size similar to that found for Kaden's problem, this effect was nevertheless tested. The results

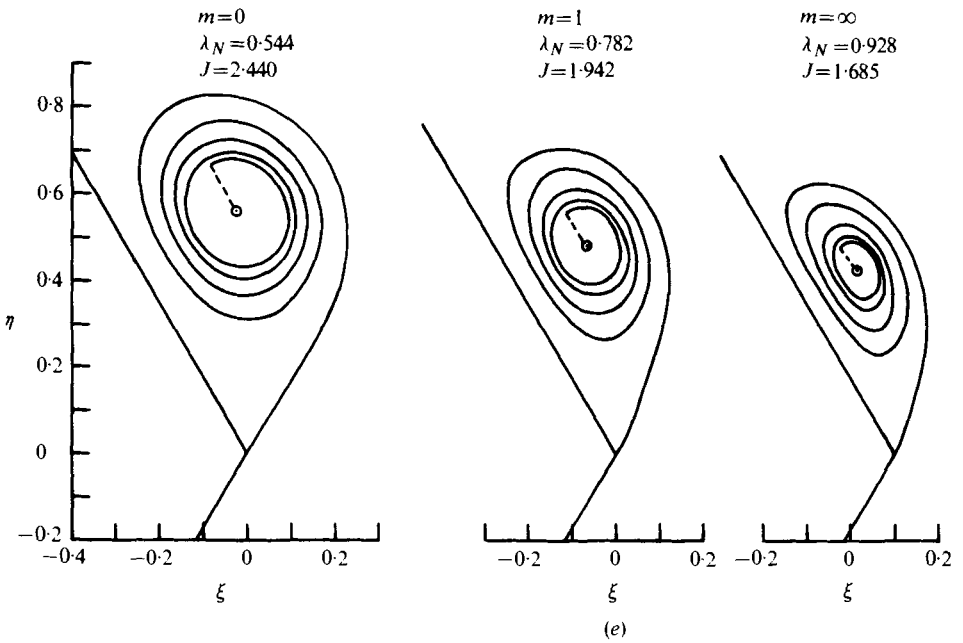

FIGURE 9. Self-similar vortex-sheet shapes in the ω plane; $N = 75$.
(a) $\beta = 0$, (b) $\beta = \frac{1}{8}$, (c) $\beta = \frac{1}{4}$, (d) $\beta = \frac{1}{2}$, (e) $\beta = \frac{3}{8}$.

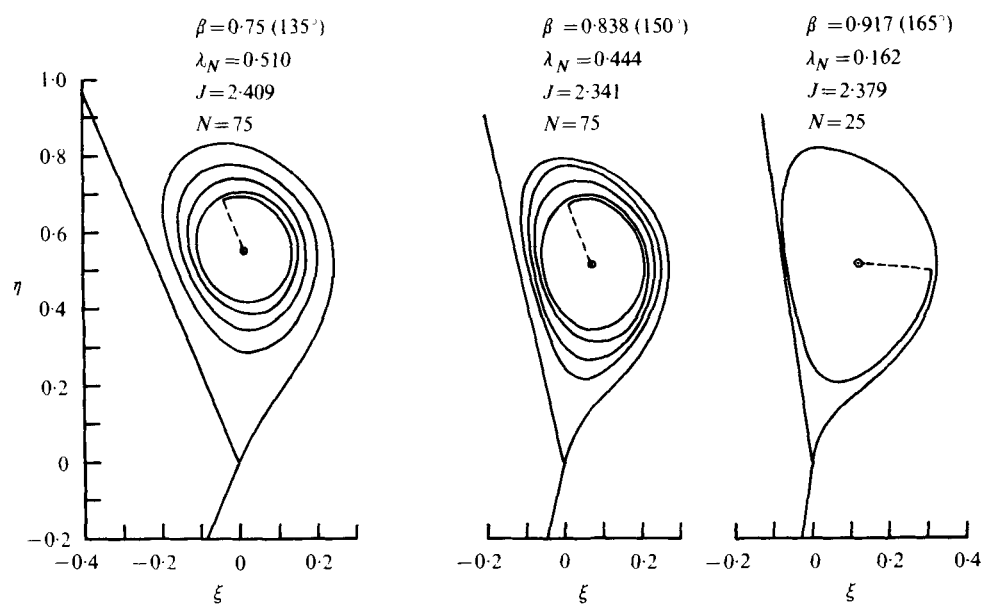

FIGURE 10. Self-similar vortex-sheet shapes in the ω plane; $m = 0$, $N = 75$.

are depicted in figures 8(*a*) and (*b*) for $m = 0$ and $\beta = 0$. Again the effect of step size appears to be small compared with the sheet spacing, and for this reason, in the sheet shapes illustrated in figures 9(*a*)–(*e*) we have drawn smooth curves through the calculated points. Note that the solutions for $m = \infty$ have no physical meaning in terms of the similarity law but represent the limiting behaviour of solutions for m greater

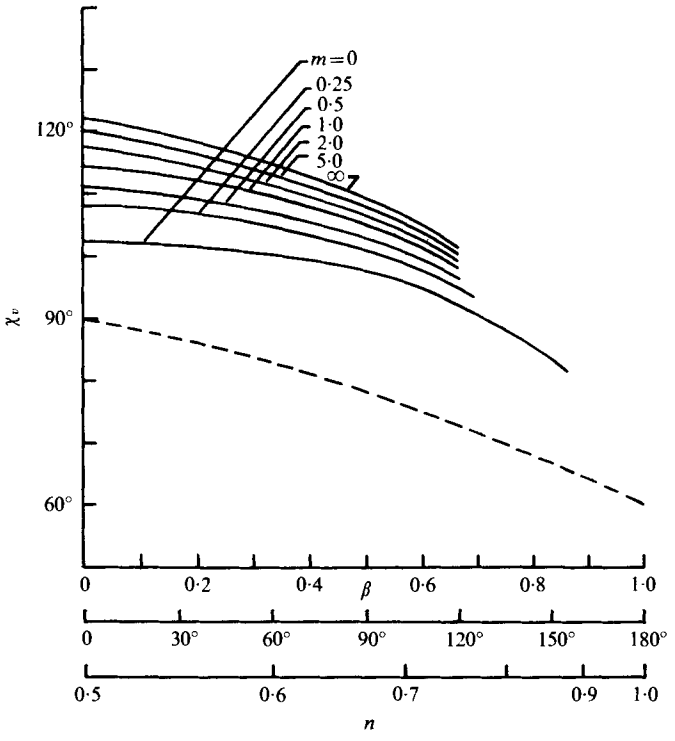

FIGURE 11. Variation of isolated vortex angle with wedge angle. ——, present; – – –, Rott (1956).

than about 10. For increasing m at constant β, figures 9(*a*)–(*e*) show that the sheet becomes more loosely wound about the spiral centre. Of the total circulation, the fraction λ_N lying on the $4\frac{1}{2}$ turns of the sheet represented in the calculations increases from about 55 % to 97–98 % as $m \to \infty$. Increasing β at constant m appears to induce increasing ellipticity in the sheet shape, although for the larger wedge angles this effect can also be associated with increasing m. For all cases where ellipticity is evident, it is noticeable that the sheet turns do not appear to become more circular towards the inner part of the solutions. Following Moore's (1975) interpretation of ellipticity for Kaden's problem and that of Smith (1968) for similar effects in the leading-edge separation problem, we might interpret this effect as the influence of the straining field produced by the attached flow and the bound circulation in the wedge on the inner parts of the spiral.

For wedge angles above 120° it was found to be increasingly difficult to obtain solutions for a given value of m, presumably because the finite-difference equations become ill conditioned in the limit $\beta \to 1$ ($n \to 1$). The maximum wedge angles for which $N = 75$ solutions could be obtained for $m = 0$, 1 and ∞ were 155°, 120° and 120° respectively, which are similar to those for which Smith (1971) could obtain solutions for the related problem of leading-edge separation from a slender delta wing of rhombic cross-section. For $m = 0$, some solutions for $N = 25$ could be found for wedge angles greater than 155°, one of which is shown in figure 10. Note in figures 9(*e*) and 10 the appearance of a point of inflexion in the sheet shape at $m = 0$ for wedge angles greater than about 120°.

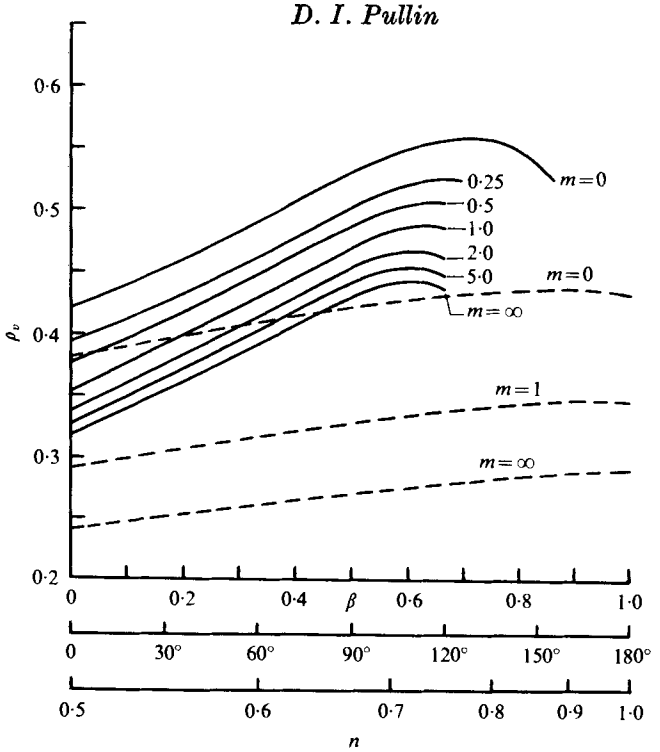

FIGURE 12. Variation of isolated-vortex radius with wedge angle. ——, present; – – –, Rott (1956).

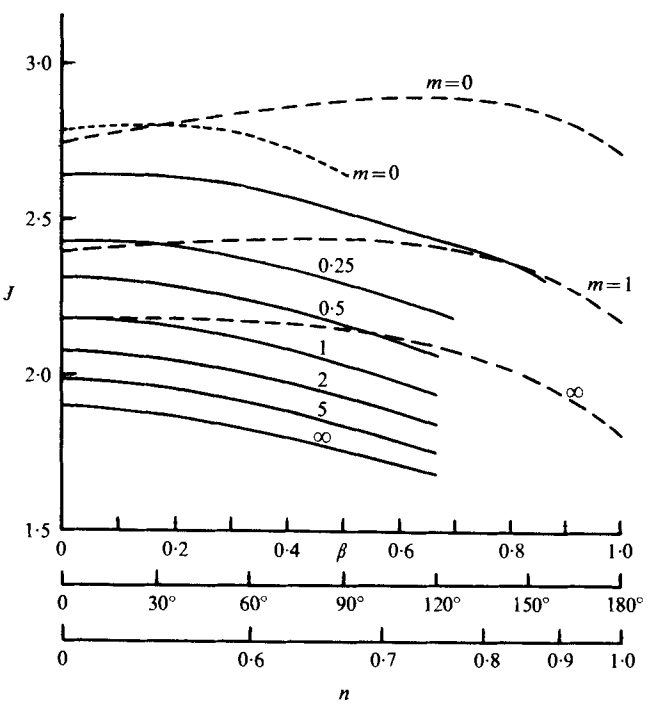

FIGURE 13. Variation of dimensionless circulation with wedge angle. ——, present; - - - -, Blendermann (1969); – – –, Rott (1956).

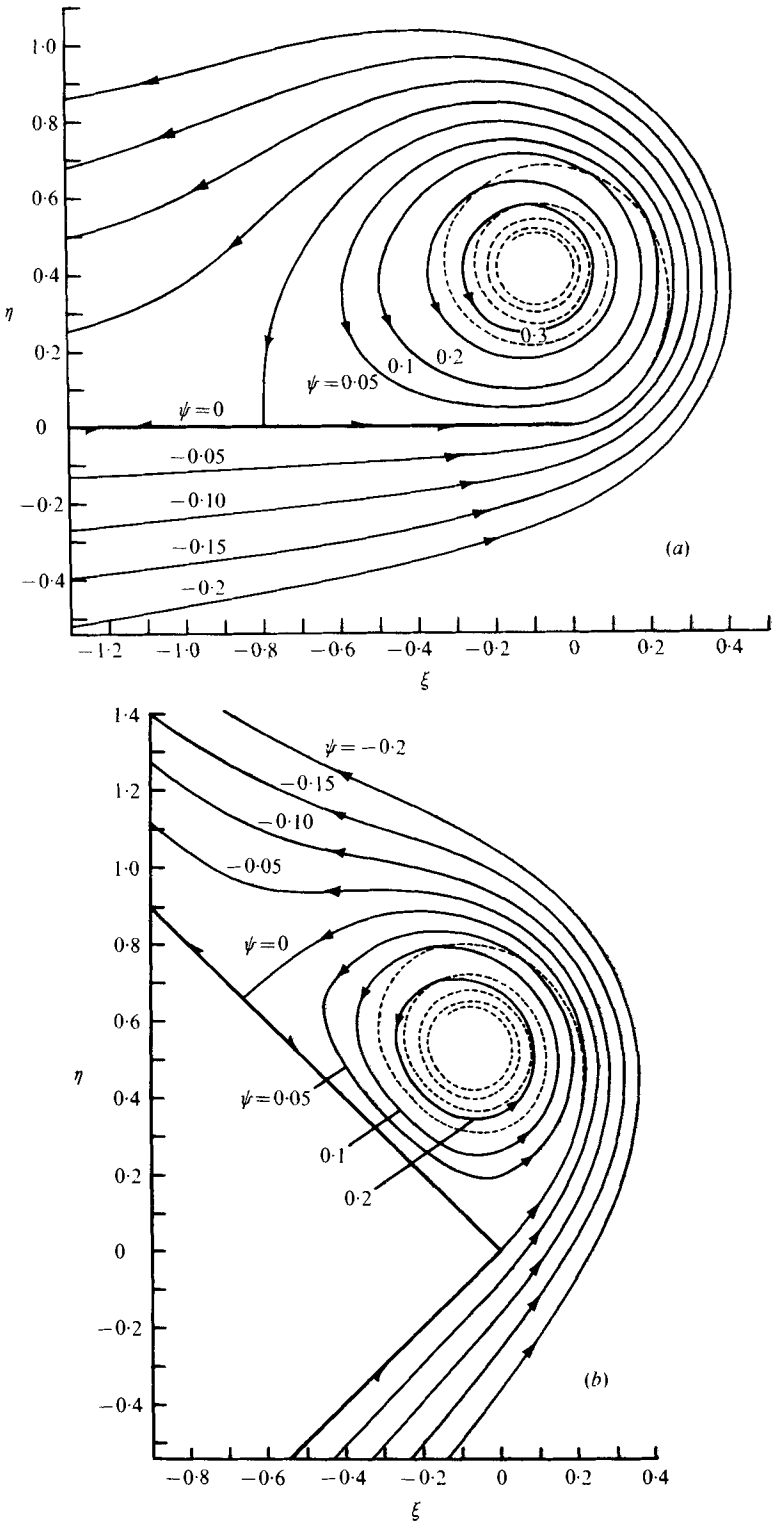

FIGURE 14. Instantaneous streamlines in the ω plane; $m = 0$. (*a*) $\beta = 0$, (*b*) $\beta = 0{\cdot}5$. ——, streamlines; – – –, vortex sheet.

In the limit $\lambda_N \to 0$, the vortex sheet vanishes and the whole solution reduces to an isolated vortex joined to the wedge apex by a cut in the ω plane. Rott's (1956) analytical solution for this limit may be written as

$$\chi_v = \frac{1}{n}\cos^{-1}\left(\frac{1}{2n^{\frac{1}{2}}}\right), \quad \rho_v = \left[\frac{[n(4n-1)]^{\frac{1}{2}}}{2[3-(2-n)/(1+m)]}\right]^{1/(2-n)}, \tag{39a,b}$$

$$J = 2\pi n^{\frac{1}{2}}\rho_v^n. \tag{39c}$$

These solutions are compared with the results of the present calculations in figures 11–13. The discrepancies between the present values of J and those obtained by Blendermann (1969) for $m = 0$ may be attributed to the fact that Blendermann appears to neglect a non-zero force on the cut in the complex plane joining ω_v to ω_N, so that his overall sheet–cut–vortex system is not approximately force free (apart from discretization errors) as in the present solutions.

Figures 14 (*a*) and (*b*) show lines of constant $\psi = \text{Im}\,\Omega$ obtained from the calculated solutions for $m = 0$, $\beta = 0$ and $m = 0$, $\beta = 0{\cdot}5$ respectively. The relationship of these curves to the actual streamlines is given by (37), which shows that lines of constant $\Psi = \text{Im}\,[W(z,t)]$ expand with the vortex sheet like a wave through the fluid with increasing time. Topologically, the pattern for $m = 0$ and $\beta = 0$ consists of a moving centre at the spiral vortex centre and a moving half-saddle point where the streamline from the flat-plate edge reattaches to the plate surface. These two features also exist for the case $m = 0$, $\beta = 0{\cdot}5$ but in addition we have what should be termed a degenerate saddle point at the wedge apex. For both cases the closed streamline $\psi = 0$ ($\Psi = 0$) might be termed an 'entrainment' boundary, since all fluid engulfed within this moving curve will end up between the turns of the rolled-up sheet and eventually as part of a rotational core and a viscous subcore. The same may be said for $\psi = 0$ in figure 4 for Kaden's problem. It is interesting to compare figure 4 with figure 14 (*a*). Both of these flows have the same (time)$^{\frac{2}{3}}$ similarity law, both may be shown to have essentially the same first-order asymptotic spiral vortex and both may be regarded as having the same initial conditions. The difference between them is the bound vortex sheet (flat plate) in the present starting-flow problem.

3.4. *Comparison with asymptotic solution*

Rott (1956) obtained a solution of (35) in the inner spiral part of the sheet ($\lambda \to 1$) which for $m < \infty$ may be written as

$$\omega - \omega_v = \alpha\tau^{-M}\exp\left[i\left(\frac{J}{2\pi C^{2-n}\alpha^2}\tau + \epsilon\right)\right], \tag{40}$$

where $\tau = (1-\lambda)^{1/(1-2M)}$ with $M = (1+m)/(2-n)$, and α and ϵ are constants to be determined. Like (21), (40) represents a tightly wound nearly circular spiral. Since it likewise does not account for effects of ellipticity in the sheet shape, it is generally rather difficult to estimate α and ϵ by patching to the numerical solution. The case $\beta = 0$ is exceptional however, as ellipticity in the sheet shape was found to be small. Hence table 1 shows values of α and ϵ for $\beta = 0$ and $m = 0$, 1 and 2 obtained by patching (40) to ω_{74} from the numerical solutions. (The case $m \to \infty$ is not included since (40) is not valid in this limit.) We again consider properties of the numerical and asymptotic solutions obtained by following a fluid-particle path. Now since all fluid particles

m	α	ϵ	J	$\lvert d\omega/d\lambda\rvert_{\lambda=0}$
0	0·419	1·81	2·640	3·90
1	0·289	0·760	2·185	1·60
2	0·256	−2·45	2·079	1·35

TABLE 1. Values of parameters in leading-order asymptotic solution obtained from numerical solutions; $\beta = 0$.

forming the sheet have at one time passed through the wedge apex, the sheet is a streakline of the flow. Consider a typical sheet material particle $\Gamma = \Gamma_0$ which passes through the apex at time t_0. From (32) it follows that for the particle path

$$t/t_0 = (1-\lambda)^{1/(1-2M)},$$

so that τ ($\geqslant 1$) in (40) may be identified with the non-dimensional time. Equations (31) and (41) then show that the fluid particle eventually moves in a circular orbit of constant radius r_0 with respect to the sheet centre and with azimuthal velocity V_θ given respectively by

$$r_0 = \alpha C a^{1/(2-n)} t_0^M, \quad V_\theta = \frac{J a^{1/(2-n)}}{2\pi\alpha C^{1-n}} t_0^{M-1}. \tag{41), (42}$$

From (41) and (42) it follows that the azimuthal velocity field obtained by replacing the irrotational flow field with discrete jumps by the smoothed-out rotational field is $V_\theta \sim r_0^{1-1/M}$. Hence V_θ is finite at the spiral centre for $m \geqslant 1-n$ and infinite otherwise. From (32) and (40) the asymptotic sheet shape may be obtained as

$$r = \alpha C a^{1/(2-n)} \left[\left(\frac{J}{2\pi\alpha^2 C^{2-n}}\right)\left(\frac{t}{\theta-\epsilon}\right)\right]^M, \tag{43}$$

from which it follows that the distance between successive sheet turns at constant radius decreases as $\delta r \sim r^{1+1/M} t^{-1}$.

From (23), (31) and (32), the sheet strength following the particle may be obtained as

$$\frac{\gamma(\tau)}{\gamma(\tau=1)} = (2M-1)\,\tau^{-(M+1)} \frac{\lvert d\omega/d\lambda\rvert_{\lambda=0}}{\lvert d\omega/d\tau\rvert}. \tag{44}$$

Using (40), for large τ this becomes to leading order

$$\frac{\gamma(\tau)}{\gamma(1)} = \frac{2\pi(2M-1)\,\alpha C^{2-n}}{J} \left|\frac{d\omega}{d\lambda}\right|_{\lambda=0} \tau^{-1}, \tag{45}$$

which, as for Kaden's problem, corresponds to sheet stretching with γ decreasing at all points on the sheet as $\gamma \sim \Gamma_0^{(1+m)/(n+2m)} t^{-1}$ for all $\beta < 1$, $m < \infty$. However, the numerical solutions obtained from (44) lead to rather different behaviour, as may be seen in figures 15(*a*)–(*c*), where they are compared with (45) for the parameter values in table 1. Except for $\beta = 0$ and $m = 0$, the present calculations predict that, following a particle, the sheet undergoes a sequence of alternate stretching and compression processes superimposed upon an overall stretching. The amplitude of the oscillations seems to increase with increasing m and β and to decrease only slowly with increasing τ. By computing the actual particle trajectories (not shown) it was found that the minima in the sheet strength correspond to points at which the particle moves roughly normal to the wedge upper surface, while the maxima correspond to points

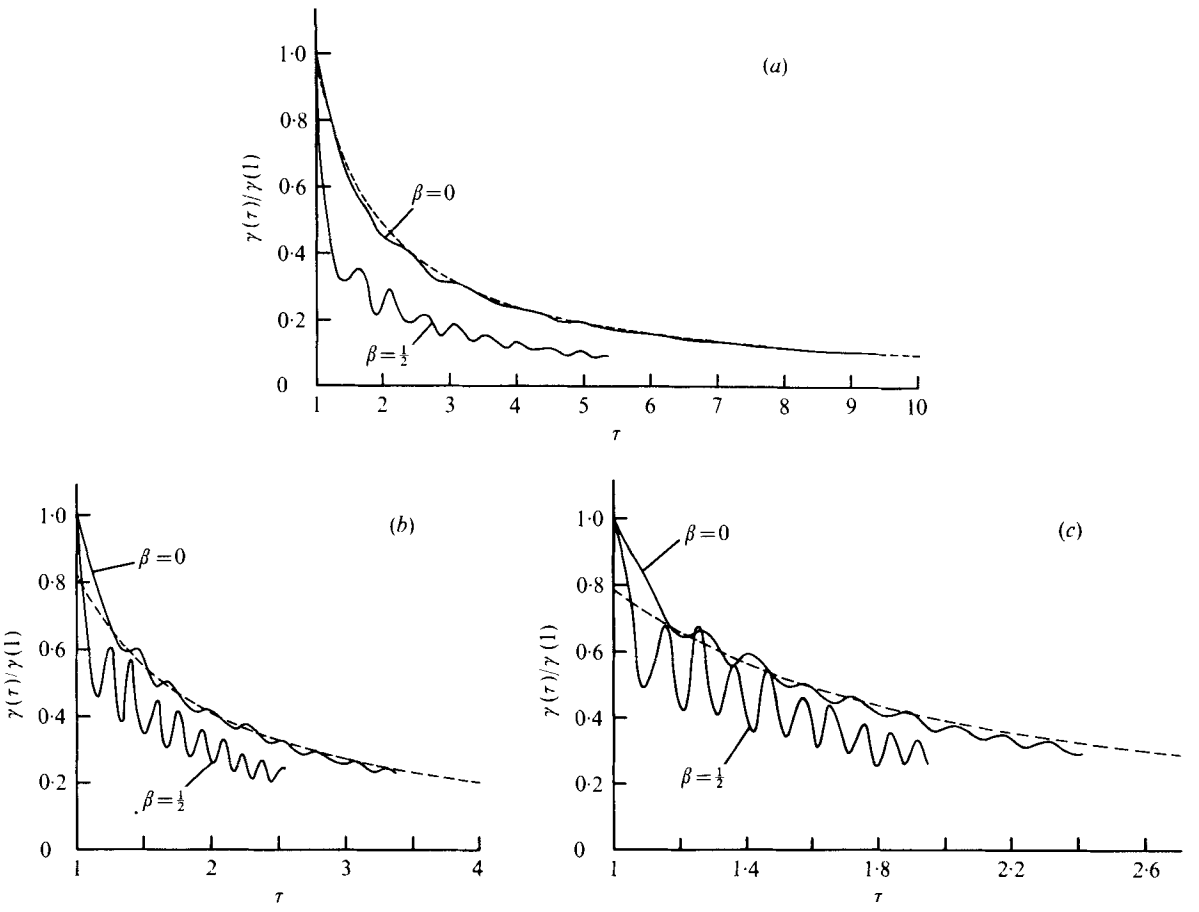

FIGURE 15. Variation of vortex-sheet strength with dimensionless time following a fluid particle. (*a*) $m = 0$, (*b*) $m = 1$, (*c*) $m = 2$. ——, present calculation; – – –, asymptotic.

at which the motion is tangential to the upper surface. This oscillation has an analogy in slender-wing leading-edge flow, for which Smith (1968) found sinuous variations in the vortex-sheet strength along the sheet length. The effect is not predicted by (45) and is therefore probably associated with the straining influence of the attached flow and the wedge vortex image on the inner spiral sheet.

4. Discussion

Although there are little experimental data readily available which could be quantitatively compared with the present results, several workers have obtained interesting flow-visualization photographs of considerable qualitative relevance. Rott (1956) includes in his paper a photograph of a vortex generated by the diffraction of a shock wave by a sharp edge. In terms of the present parameters the flow corresponds to $m = 0$ and $\beta = \frac{1}{2}$ (90° wedge). Apart from drawing attention to the presence of a substantial secondary vortex (the effects of which have been neglected in the present work) Rott suggests that 'wiggles' and 'knots' which may be seen in the primary shear layer near the wedge apex may be a sheet instability phenomena. The spark

shadowgraph photographs by Pierce (1961) show what has often been interpreted as an instability effect on the outer turn of the approximately two-dimensional vortex sheet emanating from the sharp edge of an accelerating body. (For Pierce's case $\beta \simeq \frac{1}{6}$ and $m \simeq 2$ initially.) However, on the basis of having obtained and eliminated similar effects in photographs of the unsteady bilge-keel vortex on a ship model, Professor P. T. Fink of the University of New South Wales suggests (private communication) that this phenomenon may have been due to the effect of 'jitter' induced by solid friction in Pierce's experimental apparatus. Fink & Soh (1974) present a good photograph of the ship bilge-keel vortex produced by impulsive motion which shows no sign of instability. Likewise Prandtl & Tietjens' photograph gives no indication of flow instability, all of which suggests that the wiggles in Pierce's photographs may represent an apparatus-induced disturbance that does not amplify.

The stability problem for a general two-dimensional vortex sheet has been treated by Moore (1976) following earlier work by Moore & Griffith-Jones (1974). Using a short-wave approximation, Moore found that a sufficient condition for the evolution of small disturbances on the sheet to be determined by local sheet properties was that the undisturbed sheet strength be of the form $\gamma(\Gamma, t) = f(\Gamma)\, g(t)$, local sheet stretching faster than a certain rate being one stabilization mechanism. As a special case, the continuously stretching spiral sheet with equation

$$r^{2-\delta}\theta/t = \text{constant} \tag{46}$$

was shown to be stable. For Kaden's problem, (46) with $\delta = \frac{1}{2}$ corresponds to the asymptotic spiral (21) and, in view of the good agreement with the numerical solution, Moore's analysis is probably sufficient to show that the sheet is stable. Similar conclusions were reached by Fink & Soh (1977) in their numerical treatment of a finite vortex sheet with an initially elliptical circulation distribution. For the wedge starting-flow problem (43) shows that $\delta = 2 - 1/M$. Here, however, the present solutions show regions of local sheet compression, which is presumably a sheet destabilization effect and which is absent from the asymptotic result. Moreover, it may be shown from the solutions that Moore's sufficient condition for the validity of the local stability theory may be significantly violated, so that it is generally difficult to infer stability of the full solution from stability of the (first-order) asymptotic solution. A possible exception is the case $m = 0$, $\beta = 0$ (which corresponds to Fink & Soh's photograph), for which figure 15(*a*) shows fairly small oscillations in γ and good agreement with the asymptotic solution. Clearly the stability question for other cases is a rather complex one. Further experimental evidence and properly unsteady calculations of the sheet motions which include nonlinear stability effects will be required before it can be finally resolved.

5. Conclusions

For the problem of the roll-up of an initially plane semi-infinite vortex sheet, the present calculations indicate that elliptical distortions in the shape of the rolled-up portion of the sheet are small. After the few initial turns the sheet shape appears to be well approximated by Kaden's nearly circular asymptotic spiral. Following a fluid particle, the continuous sheet stretching with a (time)$^{-1}$ variation in the local sheet strength predicted by the Kaden solution was found to agree substantially with the

numerical results. Application of the stability analysis of Moore (1976) to this result then shows that the sheet may be stable to small disturbances. For the self-similar wedge starting flow, the sheet is an approximately circular spiral for the flat-plate case. However, for non-zero wedge angles, elliptical distortions become very pronounced and do not appear to decrease substantially over the inner turns of the calculated solutions. Moreover, with the exception of impulsively started flow past a flat plate, the sheet strength following a fluid particle was found to undergo a cyclic stretching/compression process, in some cases with large amplitude. Since neither of these effects are predicted by the leading-order asymptotic solution it is concluded that they are both the result of straining of the sheet spiral induced by the attached flow and the bound circulation in the wedge. The influence of this rather complicated sheet behaviour on sheet stability remains an unanswered question.

The author wishes to thank Dr A. E. Perry for several valuable discussions.

Appendix A. The behaviour of the sheet near the wedge apex

To obtain the leading-order solution for the sheet behaviour near the leading edge for $\beta > 0$, we use (36) to write (35) in a form suggested by Rott (1956) in which the velocity field for each element of the sheet is paired with that due to its image in the wedge together with sufficient of the attached flow to give a finite velocity at the wedge apex, viz.

$$(1-n)\,[\bar{\omega}+Q(1-\lambda)\,d\bar{\omega}/d\lambda] = nJ\omega^{2n-1}G(\omega), \tag{47a}$$

where

$$G(\omega) = \frac{1}{2\pi i}\mathrm{P}\int_0^1 \left[\frac{1}{\omega'^n(\omega^n-\omega'^n)} - \frac{1}{\bar{\omega}'^n(\omega^n+\bar{\omega}'^n)}\right] d\lambda'. \tag{47b}$$

For $n = \frac{1}{2}$ ($\beta = 0$) the solution of (47) near $\lambda = 0$ takes the form (Rott 1956)

$$\omega = K_1\lambda + iK_2\lambda^{\frac{3}{2}} + \text{higher-order terms}, \tag{48}$$

where K_1 and K_2 are real constants which depend on the overall flow.

For $n > \frac{1}{2}$ ($\beta > 0$), (48) is no longer valid and the solution takes on a different character. We require a solution valid to first order, which we assume is of the form

$$\omega = K\lambda^{\mu} + \text{higher-order terms}, \tag{49}$$

where K is a complex constant and $\mu > 0$. In the integral on the right-hand side of (47b), the first term represents a Cauchy principal value but the second term does not. By taking a point ω on the sheet very near the wedge apex, the behaviour of both of these integrals may be obtained from the results of Muskhelishvili (1946, chap. 4) for the behaviour of Cauchy-type integrals on and near the ends of the line of integration.

Putting $\nu = \mu n$ and using (49), it turns out that for $n > \frac{1}{2}$, provided that $2-1/\nu > 0$,

$$G(\omega) = -\frac{\omega^{n(1/\nu-2)}}{2i\nu}\left\{\cot[(2-1/\nu)\pi]\left(\frac{1}{K^n}\right)^{1/\nu} - \frac{\exp[-(2-1/\nu)\pi i]}{\sin[(2-1/\nu)\pi]}\left(\frac{-1}{\bar{K}^n}\right)^{1/\nu}\right\} + G^*(\omega), \tag{50}$$

where $\omega^{n(2-1/\nu)}G^*(\omega) \to 0$ for $\omega \to 0$. Substituting this result into (47a), using (49) and

equating powers of leading order in λ leads to $\nu = n$ ($\mu = 1$), which satisfies $2 - 1/\nu > 0$ for $n > \frac{1}{2}$, and also to

$$K = [J/2(1-n)Q]^{\frac{1}{2}} e^{\frac{1}{2}i\beta\pi}. \tag{51}$$

Substituting into (50) gives

$$G(\omega) = \frac{\omega^{1-2n}}{2n}\left[\frac{2(1-n)Q}{J}\right]^{\frac{1}{2}} \exp\left(\frac{-i(2n-1)\pi}{2n}\right) + G^*(\omega). \tag{52}$$

Since both sides of (47a) are equal to $d\Omega/d\omega$ on the sheet, substitution of (52) and use of the Plemelj formulae gives the non-dimensional complex velocities on the windward ($-$) and leeward ($+$) sides of the sheet near the apex as

$$(d\Omega/d\omega)_+ = nJ\omega^{2n-1}G^*(\omega), \tag{53a}$$

$$(d\Omega/d\omega)_- = [2(1-n)QJ]^{\frac{1}{2}} \exp[-i(2n-1)\pi/2n] + nJ\omega^{2n-1}G^*(\omega). \tag{53b}$$

From (53) it follows that the leeward side of the wedge is a stagnation point while the non-dimensional speed on the windward side is $[2(1-n)QJ]^{\frac{1}{2}}$. The leading-order solution for small λ is

$$\omega = [J/2(1-n)Q]^{\frac{1}{2}} \exp[i(2n-1)\pi/2n]\lambda + \ldots, \tag{54}$$

which is sufficient to show that the sheet leaves the wedge tangential to the windward surface as predicted by several authors. Equation (48) may be similarly established as a formal solution to (47) for $n = \frac{1}{2}$ ($\beta = 0$), with in this case $G(\omega) = a + b\omega^{\frac{1}{2}} + \ldots$ for small ω.

The qualitative difference between (54) and (48) for $n = \frac{1}{2}$ is that in the latter case the solution is determined wholly by the outer flow while for $\beta > 0$ the leading-order solution is determined locally, only weakly depending on the overall flow through J. This appears to resolve, at least mathematically, the difficulty raised by Rott (1956) regarding the existence of a near-leading-edge solution for $n > \frac{1}{2}$, namely that the sheet element immediately adjacent to the wedge apex must provide the mean velocity as well as the velocity difference across the sheet while for $n = \frac{1}{2}$ the mean velocity is provided by the outer flow, the apex element producing only the velocity difference. However, the difficulty is a purely formal one with no physical meaning since for $n > \frac{1}{2}$ the mean flow is produced not by the near-apex circulation element itself in the sense of the Biot–Savart formula, but through the rather different resolution of the attached flow singularity for $n = \frac{1}{2}$ and $n > \frac{1}{2}$. In other words the pairing of sheet and image circulation elements with the attached flow implied in (47) takes on a rather different character in these two cases.

To obtain information about both the form of the velocity field near $\omega = 0+$ and the sheet curvature at the apex would require a solution to higher order than has been given here. For the related case of the near-apex behaviour of the conical vortex sheet emanating from a slender wing of rhombic cross-section, a solution of this kind has been given by Clapworthy & Mangler (1974), who used conformal mapping methods.

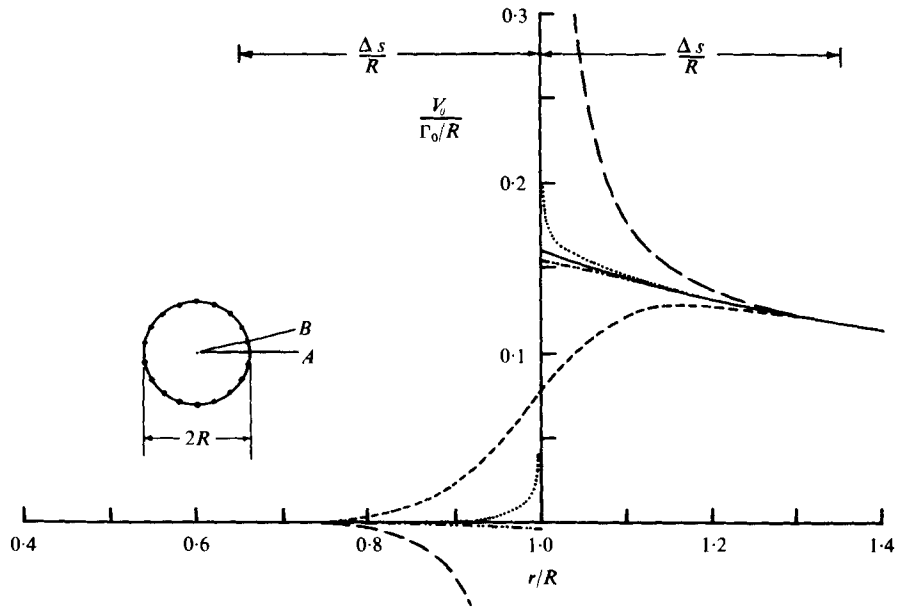

FIGURE 16. Tangential velocity field of a circular vortex sheet of radius R. ——, exact; - - - -, line A, trapezoidal rule, $N = 18$; – – –, line B, trapezoidal rule, $N = 18$; —·—·—, line A, segmented sheet with distributed circulation; · · · · ·, line B, segmented sheet with distributed circulation.

Appendix B. Velocity field of a circular vortex sheet

As a test of the accuracy of the trapezoidal rule used in the evaluation of the integrals in (12a), the velocity field due to a circular vortex sheet of constant circulation per unit length was calculated. This is a good test case for two reasons. First, the exact velocity field is known, and second, it is related to the asymptotic spiral vortex since the velocity field of the latter is approximately equivalent to an infinite set of distinct uniform concentric vortex sheets (ellipticity effects are regarded as of second order here).

Consider the complex velocity

$$\frac{dW}{dz} = \frac{1}{2\pi i}\oint \frac{d\Gamma}{z - z(\Gamma)} \tag{55}$$

at a point in the z plane due to a circular two-dimensional vortex sheet

$$z(\Gamma) = R\exp(2\pi i\Gamma/\Gamma_0)$$

of radius $r = R$ and total circulation Γ_0. The integral on the right-hand side of (55) may be evaluated exactly to yield for the radial and tangential velocity fields

$$\frac{V_r}{\Gamma_0/R} = 0, \tag{56}$$

$$\frac{V_\theta}{\Gamma_0/R} = \begin{cases} 0 & (r < R), \quad (57a) \\ \dfrac{1}{2\pi}\left(\dfrac{R}{r}\right) & (r > R). \quad (57b) \end{cases}$$

Approximating the circular vortex sheet by N equal straight-line segments joined at $z_n/R = \exp[i\pi(2n-1)/N]$ $(n = 1, \ldots, N)$ and evaluating the integral on the right side by the trapezoidal rule yields

$$\frac{dW/dz}{\Gamma_0/R} = \frac{R}{2\pi i N} \sum_{n=1}^{N} (z - z_n)^{-1}. \tag{58}$$

An alternative, more sophisticated approximation may be obtained by assuming a linear variation of $z(\Gamma)$ with Γ between each pair of points (z_{n-1}, z_n) and integrating over each of the N segments to obtain

$$\frac{dW/dz}{\Gamma_0/R} = \frac{R}{2\pi i N} \sum_{n=1}^{N} (z_n - z_{n-1})^{-1} \log\left[\frac{z - z_{n-1}}{z - z_n}\right], \tag{59}$$

where $z_0 \equiv z_N$. In figure 16 we compare $V_\theta(\Gamma_0/R)^{-1}$ evaluated from (58) and (59) along two radial lines in the z plane with (57). Here we used the value $N = 18$, which corresponds approximately to the sheet step size used in the present calculations, so that $\Delta s/R \simeq \frac{1}{9}\pi$. The two lines chosen were $z = r$ (line A), which bisects a sheet segment, and $z = r\exp(i\pi/N)$ (line B), which passes through z_1, as these represent extreme cases. Equation (59) leads to small errors at all points along line A and correctly simulates the tangential velocity discontinuity at the sheet. Along line B, (59) is logarithmically singular near z_1 but errors are otherwise small. The errors for (58) are negligible for distances from the sheet larger than $\Delta s/R$. Close to the sheet they are large but right at the sheet the Cauchy principal value is accurately represented. For points at equal distances on either side of the sheet however, the errors are of opposite sign and of approximately equal magnitude. Hence for a series of closely spaced concentric sheets, provided that the sheet-segment joints are positioned radially (as was approximately the case in the present calculations), the trapezoidal representation of the velocity field will be reasonably accurate even for sheet spacings $\delta r/\delta s < 1$ owing to error cancellation. This may partly explain the unexpected insensitivity to step size observed in the present calculations. Note that the use of distributed sheet segments as in (59) is generally much less convenient than use of the simple trapezoidal rule.

REFERENCES

Anton, L. 1939 Ausbildung eines Wirbles an der Kante einer Platte. *Ing. Arch.* **10**, 411–427. (English trans. *N.A.C.A. Tech. Memo.* no. 1398 (1956).)

Batchelor, G. K. 1970 *An Introduction to Fluid Dynamics*. Cambridge University Press.

Blendermann, W. 1969 Der Spiralwirbel am translatorisch bewegten kreisbogenprofilen Struktur, Bewegung und Reaktion. *Schiffsteck.* **16**, 3–14.

Clapworthy, G. J. & Mangler, K. W. 1974 The behaviour of a conical vortex sheet on a slender delta wing near the leading edge. *R.A.E. Tech. Rep.* no. 74150.

Fink, P. T. & Soh, W. K. 1974 Calculation of vortex sheets in unsteady flow and applications in ship hydrodynamics. *Univ. New South Wales, School Mech. Indust. Engng Rep.* Nav/Arch 74/1.

Fink, P. T. & Soh, W. K. 1978 *Proc. Roy. Soc.* A (in press).

Guiraud, J. P. & Zeytounian, R. Kh. 1977 A double-scale investigation of the asymptotic structure of rolled-up vortex sheets. *J. Fluid Mech.* **79**, 93–112.

Kaden, H. 1931 Aufwicklung einer unstabilen Unstetigkeitsfläche. *Ing. Arch.* **2**, 140. (English trans. *R.A. Lib. Trans.* no. 403.)

MOORE, D. W. 1974 A numerical study of the roll-up of a finite vortex sheet. *J. Fluid Mech.* **63**, 225–235.

MOORE, D. W. 1975 The rolling up of a semi-infinite vortex sheet. *Proc. Roy. Soc.* A **345**, 417–430.

MOORE, D. W. 1976 The stability of an evolving two-dimensional vortex sheet. *Mathematika* **23**, 35–44.

MOORE, D. W. & GRIFFITH-JONES, R. 1974 The stability of an expanding vortex sheet. *Mathematika* **21**, 128–133.

MOORE, D. W. & SAFFMAN, P. G. 1973 Axial flow in laminar trailing vortices. *Proc. Roy. Soc.* A **333**, 491–508.

MUSKHELISHVILI, N. 1946 *Singular Integral Equations* (trans. J. M. R. Radok). Noordhoff.

PERRY, A. E. & FAIRLIE, B. D. 1974 Critical points in flow patterns. *Adv. in Geophys.* **18**, 299–315.

PIERCE, D. 1961 Photographic evidence of the formation and growth of vorticity behind plates accelerated from rest in still air. *J. Fluid Mech.* **11**, 460–464.

PULLIN, D. I. 1975 Calculations of the steady conical flow past a yawed slender delta wing with leading edge separation. *Aero. Res. Counc. R. & M.* no. 3767.

ROTT, N. 1956 Diffraction of a weak shock with vortex generation. *J. Fluid Mech.* **1**, 111–128.

SMITH, J. H. B. 1966 Theoretical work on the formation of vortex sheets. *Prog. in Aero. Sci.* vol. 7 (ed. D. Kuchemann), pp. 35–51. Pergamon.

SMITH, J. H. B. 1968 Improved calculations of leading edge separation from slender delta wings. *Proc. Roy. Soc.* A **306**, 67–90.

SMITH, J. H. B. 1971 Calculations of the flow over thick, conical slender wings with leading edge separation. *R.A.E. Tech. Rep.* no. 71057.

SMITH, J. H. B. 1972 Similar solutions for slender wings with leading edge separation. Paper presented at the *13th Int. Cong. Theor. Appl. Mech., Moscow.*

WEDEMEYER, E. 1961 Ausbildung eines Wirbelpaares an den Kanten einer Platte. *Ing. Arch.* **30**, 187–200.